Diffusion of the Vertical Field into the Tape-Wound Magnet

N. Gottardi[+], F. Mast
H. Preis, R. Süß

IPP 1/189 July 1981

MAX-PLANCK-INSTITUT FÜR PLASMAPHYSIK
8046 GARCHING BEI MÜNCHEN

MAX-PLANCK-INSTITUT FÜR PLASMAPHYSIK

GARCHING BEI MÜNCHEN

Diffusion of the Vertical Field into the Tape-Wound Magnet

N. Gottardi[+], F. Mast

H. Preis, R. Süß

IPP 1/189 July 1981

[+] Gast aus dem Istituto di Macchine-Politecnico di Milano

Die nachstehende Arbeit wurde im Rahmen des Vertrages zwischen dem Max-Planck-Institut für Plasmaphysik und der Europäischen Atomgemeinschaft über die Zusammenarbeit auf dem Gebiete der Plasmaphysik durchgeführt.

IPP 1/189 N. Gottardi[+]
F. Mast
H. Preis
R. Süß

Diffusion of the Vertical Field into the Tape-Wound Magnet

July 1981 (in English)

Abstract

Magnetic field diffusion processes in fusion experiments are investigated experimentally and numerically. For this purpose a computer program was developed to calculate eddy currents in electrically conducting structures of general geometry in order to determine their magnetic fields. The program is based on the finite element network method (FEN), in which the structure considered is divided into directed, finite elements. Each element is then treated as a branch of a three-dimensional RL network. After R and L in all of the network branches have been calculated, the network differential equations represented in matrix form is solved. The time behaviour and distribution of the eddy currents then follow directly from the solution vector of the transient branch currents.

The FEN is tested in the case of vertical field diffusion through the toroidal field coils of ZEPHYR. For this purpose an electrical model of the coil configurations was constructed on a scale of 1:5. The scaling laws applied are described. A detailed description of the measuring method used is given. The results of the calculations and measurements are compared for various frequencies of the vertical field.

[+)]Guest from Istituto di Macchine-Politecnico di Milano

Contents

1. Introduction

Investigation of the physical properties of a mainly α-particle-heated plasma was to be the principal aim of the ZEPHYR experiment. It was intended to achieve the ignited plasma state by adiabatic compression of a plasma preheated ohmically and by neutral injection /1/. First the plasma is built up by ohmic and additional neutral injection heating in a region of relatively small toroidal magnetic field (TF field).

This not ignited plasma serves as the starting point for the adiabatic compression. By increasing the vertical equilibrium field (B_V field), the plasma is shifted towards the high field region of the toroidal field magnet (TF magnet), resulting in increased plasma pressure. To get ignition conditions, e.g. primarily high plasma temperature, the compression time of the plasma should be shorter than or at least in the same range as its energy confinement time T_E. The B_V field therefore has to be raised while changing the plasma from its uncompressed to its compressed state to a value twice as large as before /2/ in a rise time $t_r \lesssim T_E = 100 \times 10^{-3}$ s. With regard to power consumption limitations of the poloidal and vertical magnetic field systems and to problems of diffusion of the B_V field into the TF magnet the lower limit of the rise time of B_V was chosen as $t_r = 100 \times 10^{-3}$ s.

The use of adiabatic compression of the plasma in ZEPHYR calls for horizontally elongated cross-sections of the vacuum vessel and the TF magnet (Fig. 1 a, 1 b). The favourite concept for the TF magnet was the so-called "tape-wound" magnet /3/, which minimizes the bending moments at the throat of the TF magnet by using conductor tapes of copper clad on tapes of cold-rolled stainless steel.

To reach a sufficiently long flat-top time of the TF field, liquid nitrogen cooling of the TF magnet is used (inertial cooling). For the same reasons the OH and VF coils are cooled down to liquid nitrogen temperature at the beginning of the current

pulse, too. Flat-top times of 7s or even longer can therefore be achieved without any external cooling during the shot.

During each regular experimental run transient eddy currents in most electrical conductors will be induced by time varying toroidal and poloidal magnetic fields. These eddy currents generate stray fields that may influence the plasma behaviour and interact mutually and with the external magnetic fields, resulting in electromagnetic forces. In the case of a hard plasma disruption when the plasma current decays in an anomalously short time interval these forces may reach critical values.

Among the most important transient phenomena associated with eddy currents on the components of an ignition tokamak will be the following:

- Hard plasma disruption if the plasma current decays in a time interval equal to or even shorter than the toroidal time constant of the vacuum vessel. The resulting electromagnetic forces on it are the dominant ones and govern the design of the vacuum vessel /4/.
- During the electrical break down phase of the plasma mostly the toroidal eddy currents on the vacuum vessel generate stray fields that may prevent breakdown of the plasma.
- Adiabatic compression of the plasma calls for a fast rising VF field, resulting in considerable stray fields[2]. They may cause delay of the B_V field buildup inside the TF magnet coupled with a serious distortion of the field geometry of B_V. The latter may diminish the stability of the plasma against vertical displacements.

  Electrical feedback systems for controlling the vertical and horizontal plasma position may also suffer a critical delay between the control current through the feedback coils and the magnetic guide field inside the TF magnet[2].

---

[2] It is supposed that the VF and feedback coils of DT burning machines are situated outside the TF magnet for remote repairing and maintenance.

Theinfluences of the different eddy current phenomena mentioned above were estimated for ZEPHYR first by rather simple analytical calculations. Especially for the penetration of the B_V field through the TF magnet the results of these estimations lead one to expect serious distortion of the B_V field during adiabatic compression of the plasma, as is shown later.

Analytical estimates of the penetration of B_{V_Z} through the tape-wound TF magnet of ZEPHYR are given in Sec. II of this report. Experimental investigation of the diffusion problem in an electrical model of the TF magnet are described in Sec. III, while the methods and some results of a new FE network code are represented in Sec. IV. The theoretical and experimental results are compared and discussed together in Sec. V. The main goalof this work was to check the FE network code for its practicability in complicated structures in tokamaks systems, as the TF magnet of ZEPHYR would be, and to prove the accuracy of its results. As a result nearly every problem of magnetic field diffusion through the components of a tokamak system can be treated with the 3 D Fe network code presented later.

2. Analytical estimate of B_V diffusion

During plasma compression the time varying B_V field excites saddle currents on the TF coils that are mainly responsible for the delay of B_V owing to their stray fields. These saddle currents form the current mode with the largest time constant denoted as ground mode and are schematically represented in Fig. 2.

Since the stray field of the ground mode dominates in most regions inside the vacuum vessel, the time behaviour of the vertical component B_{V_Z} of B_V can be approximately described by a simple transfer function inside the TF magnet[1]:

$$Z(s) = f_0(\vec{r}) + [1 - f_0(\vec{r})][1 + \tau \cdot s]^{-1} \qquad (1)$$

with $f_0(\vec{r})$ = spontaneous part of B_{V_Z}

τ = time constant of saddle currents.

The response of B_{V_Z} to a linearly rising current in the VF coils follows from eq. 1:

$$B_{V_Z}(t) = \alpha(\vec{r}) \cdot t + \alpha(\vec{r})\,[1 - f_0(\vec{r})] \cdot [e^{-t/\tau} - 1] \cdot \tau \qquad (2)$$

The term $\alpha \cdot t$ describes B_{V_Z} (t) as it would be without TF coils, and $\alpha(\vec{r})$ is a local function. In the limit $t \gg \tau$ the time dependence of B_{V_Z} simplifies to

$$B_{V_Z}(t) = \alpha(\vec{r})\,[t - (1 - f_0(\vec{r}))] \cdot \tau] \qquad (3)$$

and the time constant τ_0 of the vertical field diffusion into the TF magnet can be derived from eq. 3:

$$\tau_0 = \tau\,[1 - \langle f_0(\vec{r}) \rangle] \qquad (4)$$

It is possible to estimate τ_0 and $f_0(\vec{r})$ for the real toroidal geometry of ZEPHYR by adapting expressions given in /5/ for cylindrical geometry with an equivalent radius r_m that represents the poloidal cross-section of the TF magnet /3/:

$$\frac{r_m}{2} = \frac{\text{POL. cross-section of the TF magnet}}{\text{POL. circumference of the TF magnet}} \qquad (5)$$

The spontaneous part $\langle f_0(\vec{r}) \rangle$ of B_{V_Z} can be approximated by using eq. 5:

$$[f_0(\vec{r})]^{-1} = 1 + \frac{D}{2 \cdot r_m} \cdot \frac{1}{(1 - \ell/L)} + \frac{L}{\pi \cdot r_m} \cdot \ln \frac{0.7}{(1 - \ell/L)} \qquad (6)$$

with $L(\vec{r}) = 2 \cdot \pi \cdot R / n_p$

R = major radius

---

[1] Z(S) can be derived from an electrical equivalent circuit consisting of two resistances and one inductance.

n_p = number of TF coils

$L - \ell$ = gap between two TF coils in toroidal direction

D = thickness of copper of a TF coil.

Only the copper windings of the TF magnet have to be considered here. The casings of the TF coils and the stainless-steel part of the conductor tapes exert a negligible influence on the B_V diffusion because of their high resistivities.

The time constant τ_D of the diffusion of B_{V_Z} can be written as /3/

$$\tau_D = \frac{\mu_0}{48 \cdot \varrho} \cdot \frac{V_{Cu}}{V_M} \cdot \ell^2 \quad , \tag{7}$$

ϱ = resistivity of copper

V_{Cu} = volume of copper of the whole TF magnet

V_M = volume of TF magnet.

τ_D was estimated for the tape-wound magnet of ZEPHYR with eq.7 as

$$\tau_D = 63 \times 10^{-3} \ s \quad ;$$

using the resistivity of copper at LN_2 temperature:

$$\varrho_{Cu} = 0.25 \times 10^{-8} \ \Omega m .$$

The spontaneous part $\langle f_0(\vec{r}) \rangle$ of B_{V_Z} was estimated with eq. 6, yielding, for instance,

at R = 1.35 m $\quad f_0 = 0.68$,

and at R = 2.02 m $\quad f_0 = 0.84$.

The time constant τ of the saddle currents on the TF coils can be derived from eq. 4 together with eq. 6

$$\tau = 260 \times 10^{-3}\ s$$

Such simple estimates as derived for the B_{V_Z} component cannot be made for the horizontal component B_{V_R} of B_V for two reasons. Firstly, the B_{V_R} components are much smaller than the changes of the B_{V_Z} components caused by the eddy currents during adiabatic compression. Secondly, the time constant τ of the saddle currents is larger than the rise time of B_V. Large changes of B_{V_R} are therefore expected which may even surpass the equilibrium values of B_{V_R} and may critically alter the vertical field index. The delay τ_D in the build-up of B_{V_Z} can be tolerated owing to the large spontaneous part f_0 and can be compensated by overloading the VF coils. Whether the field index will critically be changed or not during adiabatic compression or whether feedback stabilization does really work cannot be decided by analytical estimates. Either FE calculations or measurements in an electrical model of the TF coils are thesuitable means of yielding sufficiently accurate results.

3. Measurements in the electrical model of the TF magnet

3.1. Scaling Laws

All electromagnetic phenomena which are described by Maxwell equations can be transformed linearly in time, space and electromagnetic quantities if the material properties do not depend on frequency or on the electric ormagnetic field strengths in the range of interest. The tensors of resistivity and of dielectric and magnetic susceptibilitiesare therefore constants which may only depend on space coordinates. The linear transformations fo space coordinates, time and frequency can be written as

$$\vec{r}^{\,*} = \alpha \cdot \vec{r} \tag{8a}$$

$$t^{*} = \Omega \cdot t \tag{8b}$$

$$v^{*} = \Omega^{-1} \cdot v \tag{8c}$$

All the transformed quantities are denoted by stars. By inserting eqs. 8 a and 8 b into Maxwell equations, several transformation laws and similarity theorems can be derived from the fact that Maxwell equations must be invariant against the transformations 8 a and 8 b / 6 / with regard to linear transformation of the electromagnetic fields $\vec{E}$, $\vec{D}$, $\vec{B}$ and $\vec{H}$:

$$E_i(\vec{r},t) = e \cdot E_i^{*}(\vec{r}^{\,*},t^{*}) \tag{9a}$$

$$D_i(\vec{r},t) = d \cdot D_i^{*}(\vec{r}^{\,*},t^{*}) \tag{9b}$$

$$B_i(\vec{r},t) = b \cdot B_i^{*}(\vec{r}^{\,*},t^{*}) \tag{9c}$$

$$H_i(\vec{r},t) = h \cdot H_i^{*}(\vec{r}^{\,*},t^{*}) \tag{9d}$$

The equation of definiton for $\vec{D}$

$$D_i(\vec{r},t) = \varepsilon_0 [\delta_{ij} + X_{ij}^{e}(\vec{r})] \cdot E_j(\vec{r},t) \tag{10}$$

is transformed with eqs. 9 a and 9 b to

$$D_i^{*}(\vec{r}^{\,*},t^{*}) = \varepsilon_0 \left[\delta_{ij} + X_{ij}^{e}\left(\frac{\vec{r}^{\,*}}{\alpha}\right)\right] \cdot E_j^{*}(\vec{r}^{\,*},t^{*}) \cdot \frac{e}{d}$$

with the result

$$e = d \tag{11a}$$

$$X_{ij}^{e*}(\vec{r}^{\,*}) = X_{ij}^{e}(\vec{r}) \tag{11b}$$

From the equation of definition for $\vec{H}$

$$B_i(\vec{r},t) = \mu_0 [\delta_{ij} + X_{ij}^{m}(\vec{r})] \cdot H_j(\vec{r},t) \tag{12}$$

together with eqs. 9 c and 9 d one gets

$$B_i^x(\vec{r}^x, t^x) = \mu_0 \left[\vartheta_{ij} + \hat{X}_{ij}^M \left(\frac{\vec{r}^x}{a} \right) \right] \cdot H_j^x(\vec{r}^x, t^x) \cdot \frac{h}{b}$$

with the results

$$h = b \qquad (13a) \qquad\qquad \hat{X}_{ij}^{M^x}(\vec{r}^x) = \hat{X}_{ij}^M(\vec{r}) \qquad (13b)$$

Faraday's law

$$\varepsilon_{ijk} \nabla_j E_k(\vec{r}, t) = - \frac{\partial}{\partial t} B_i(\vec{r}, t) \qquad (14)$$

is transformed to

$$\varepsilon_{ijk} \nabla_j^x E_k^x(\vec{r}^x, t^x) = - \frac{\partial}{\partial t^x} B_i^x(\vec{r}^x, t^x) \cdot \frac{b \cdot \Omega}{a \cdot \alpha} \qquad (14a)$$

using eqs. 8 a, 8 b, 9 a, 9 c, 11 a and 13 a.

The statement of invariance of eq. 14 yields with eq. 14 a

$$b \cdot \Omega = a \cdot \alpha \qquad (15)$$

The transformation of Ampere's law

$$\varepsilon_{ijk} \nabla_j H_k(\vec{r}, t) = \sigma_{ij}(\vec{r}) \cdot E_j(\vec{r}, t) + \frac{\partial}{\partial t} D_i(\vec{r}, t) \qquad (16)$$

yields

$$\varepsilon_{ijk} \nabla_j^x H_k^x(\vec{r}^x, t^x) = \sigma_{ij}\left(\frac{\vec{r}^x}{a} \right) E_j^x(\vec{r}^x, t^x) \cdot \frac{\alpha}{ab} + \frac{\partial}{\partial t^x} D_i^x(\vec{r}^x, t^x) \cdot \frac{\alpha \Omega}{a b} \qquad (16a)$$

The transformation of eq. 16 into eq. 16 a must be invariant, yielding

$$d \cdot \Omega = a \cdot b \tag{17a}$$

$$\sigma_{ij}^{x}(\vec{r}^{x}) = \sigma_{ij}(\vec{r}) \cdot \frac{d}{ab} \quad , \quad \varrho_{ij}^{x}(\vec{r}^{x}) = \varrho_{ij}(\vec{r}) \cdot \frac{ab}{d} \tag{17b}$$

The first similarity theorem can be derived from eqs. 15 and 17 a:

$$\alpha = \Omega \tag{18a}$$

The fransformation of electrical resistivity is deduced from eqs. 17 a and 17 b:

$$\varrho_{ij}^{x}(\vec{r}^{x}) = \varrho_{ij}(\vec{r}) \cdot \alpha \quad , \qquad \alpha = a \tag{19}$$

It immediately follows from eqs. 11a, 13a, 18a and 15 or 17 a that

$$e = d = b = h \; . \tag{20}$$

The transformation of the current density follows from eqs. 9 a and 19:

$$j_i^{x}(\vec{r}^{x}, t^{x}) = j_i(\vec{r}, t) \cdot (a \cdot b)^{-1}$$

and from Poisson's law one obtains the transformation of the electric charge density ϱ_e :

$$\varrho_e^{x}(\vec{r}^{x}, t^{x}) = \varrho_e(\vec{r}, t) \cdot (a \cdot b)^{-1} \tag{21}$$

In principle, it is possible to study any problem of electrodynamics in an electrical model by using the equations derived above. But eqs. 18 a and 19 impose severe restrictions on the choice of materials and of the scaling factors of the space coordinates and time.

Since eqs. 18 a and 19 describe the correct transformation of the displacement current $\vec{D}$, their use is indipensable for all problems of wave propagation and in cases with large capacitive currents.

The capacitive currents are negligible compared with the other eddy currents in most cases of magnetic field diffusion through electrical conductors. The omission of the displacement current in Ampère's law is therefore justified in describing the B_V diffusion through the TF magnet, especially owing to the low upper frequency limit of all transient phenomena, but the transformation laws are somewhat changed.

The transformation factors F for all electromagnetic quantities with or without consideration of the displacement current are represented in Table 1 with the notation

$$A^+(\vec{r}^x, t^x) = F \cdot A(\vec{r}, t),$$

A^+ = transformed quantity

A = original quantity.

$A(\vec{r},t)$	$\vec{B}$	$\vec{H}$	$\vec{E}$	$\vec{D}$	$\dot{\vec{D}}$	$\vec{j}$	ϱ_e	$\overleftrightarrow{X}^e$	$\overleftrightarrow{X}^M$	ϱ	$\vec{r}$	t
F $\dot{\vec{D}} \neq 0$	$\frac{1}{b}$	$\frac{1}{b}$	$\frac{1}{b}$	$\frac{1}{b}$	$\frac{1}{ba}$	$\frac{1}{ba}$	$\frac{1}{ba}$	1	1	a	a	a
F	$\frac{1}{b}$	$\frac{1}{b}$	$\frac{\alpha}{b \cdot a}$	$\frac{\alpha}{b \cdot a}$	$\frac{1}{ba} \cdot \frac{\alpha^2}{a^2}$	$\frac{1}{ba}$	$\frac{\alpha}{ba^2}$	1	1	α	a	$\frac{a^2}{\alpha}$
$\dot{\vec{D}} = 0$	$\frac{1}{b}$	$\frac{1}{b}$	$\frac{a}{b\Omega}$	$\frac{a}{b\Omega}$	$\frac{1}{ba} \cdot \frac{a^2}{\Omega^2}$	$\frac{1}{ba}$	$\frac{1}{b\Omega}$	1	1	$\frac{a^2}{\Omega}$	a	Ω

Table 1

The framed quantities in Table 1 can be chosen **independently** [1]. The number of free variables will increase from two to three if the displacement current is negligible and will considerably simplify construction of an electrical model.

But it schould be kept in mind that by using only the equations for $\dot{\vec{D}} = 0$ the capacitive currents on the original TF magnet are not accurately transferred to the model. The mismatch between the correctly transferred capacitive current j_c^* and the capacitive current j_c transferred with $\dot{\vec{D}} = 0$ is found from Table 1 to be

$$j_c = \frac{a^2}{\Omega^2} \cdot j_c^* \qquad (22)$$

and has to be checked in any case.

3.2 Electrical model of the TF magnet

The parameters of the electrical model of the tape-wound magnet were fixed with the transformation factors for $\dot{\vec{D}} = 0$. Three factors F of Table 1 can therefore be chosen independently of each other.

The geometric scale factor a was chosen as a = 0.2. It is large enough to get accurate space resolution of the measurements but it is sufficiently small to limit the expense for the model and for the power supply of the VF coils to a reasonable amount.

The transformation factor of the resistivity α is given by the ratio of copper resistivities at room temperature to those at LN_2 temperature:

$$\alpha = \varrho^*/\varrho = \varrho(293\,°K)/\varrho(80\,°K) = 6.9$$

[1] For $\dot{\vec{D}} \neq 0$ the transformation factors 1/b and a can be chosen independently, whereas in the case $\dot{\vec{D}} = 0$ either 1/b, α and a or 1/b, a and Ω represent a set of free variables.

The transformation factor of the frequency Ω^{-1} can be deduced from Table 1 by the relation $\Omega^{-1} = \alpha / a^2$, yielding $\Omega^{-1} = 172.5$.

Since the VF coils of the original are also cooled down to LN_2 temperature at the beginning of the current pulse and are made from copper, like the TF coils, the same transformation factors F were used for the VF and TF coils[1]. The numbers of windings of the VF coils in the model and in the original are the same, while each TF coil of the model consists of 34 windings compared with 43 windings in the original. But the complete copper thickness of a TF coil is correctly transformed[2].

Because there is no suitable material with a resistivity 6.9 times as high as that of stainless steel at LN_2 temperature, each copper winding of the model TF coils is insulated against its neighbouring windings by 0.8 mm thick hostaphan foil which replaces the virtual model conductor of stainless steel.

Two sources of error currents may arise from this technique. The resistive currents in the stainless steel tapes are not considered in the electrical model, and the capacitive coupling between two windings will be diminished by the increased thickness of the insulating sheet. This increase of the insulator thickness between two windings of the model decreases the capacitive currents between them and counteracts the increase of the capacitive currents caused by the incorrect transformation using $\dot{\vec{D}} = 0$, which yields from eq. 22

$$a^2/\Omega^2 = 1.2 \times 10^3 .$$

It was shown that even at the highest measuring frequency these capacitive currents

---

1) During adiabatic compression the VF and TF coils remain near LN_2 temperature and the transformation factors are assumed to be independent of time.

2) The change of thickness of a single copper tape will be small compared with the complete thickness of the coil, if the number of windings is changed from 43 to 34 because of the thickness of the copper material available.

are negligible compared with the eddy currents in the copper, the eddy currents in the stainless steel tapes like-wise being negligible. Schematic drawings of the vertical (plane A-A) and meridional cross-section of the electrical model with TF coils are shown in Figs. 3 a and 3 b.

3.3 Measuring technique

Two principal measuring methods can be applied to study the diffusion of the B_V field through the TF magnet in an electrical model.

Real-time measuring requires that the VF coils of the model be supplied with a current pulse which is similar to the corresponding pulse in the original experiment and needs broad-band measuring equipment. High current pulses through the VF coils are necessary to get a sufficiently large signal-to-noise ratio of the measurements with magnetic probes. It is difficult to shape the VF current pulses in the model proportionally to those in the original and this method is therefore inflexible and cumbersome.

A second possibility is to feed the VF coils with sinusoidal currents. The resulting sinusoidal magnetic field components can be measured with narrow bandwith equipment, resulting in large signal-to-noise ratios at small supply currents through the VF coils. It is necessary to measure at different fixed frequencies across the frequency band of interest to determine the transfer function $\boldsymbol{G}\ (\vec{r}, w)$ of the TF magnet. Once $\boldsymbol{G}(\vec{r}, w)$ is determined, it is possible by Fourier synthesis to simulate the behaviour of $\vec{B}_V\ (\vec{r}, t)$ as a response to a large variety of current pulses $\boldsymbol{I_V}\ (t)$ through the VF coils. The investigation of B_V diffusion through the TF magnet was conducted by the method of measuring Fourier components and is described in the following.

The 6 VF coils of the model (Fig. 3 a) are series connected and are supposed to be supplied by a current

$$I_V(t) = \frac{1}{2\pi} \cdot \int_{-\infty}^{+\infty} I_V(\omega) \cdot e^{i\omega t}\, d\omega . \qquad (23)$$

without the TF coils, $I_V(t)$ generates a vertical magnetic field $\vec{B}_V^{\,0}(\vec{r}, t)$ with the Fourier-transformed components

$$B^0_{V_{R,Z}}(\vec{r},t) = f_{R,Z}(\vec{r}) \cdot I_V(t) = \frac{1}{2\pi} \cdot \int_{-\infty}^{+\infty} B^0_{V_{R,Z}}(\vec{r},\omega) \cdot e^{j\omega t}\, d\omega \quad (24)$$

with $$B^0_{V_{R,Z}}(\vec{r},\omega) = f_{R,Z}(\vec{r}) \cdot I_V(\omega) \,. \quad (25)$$

The vertical component of B_V^0 is denoted by $B^0_{V_Z}$, and the horizontal component by $B^0_{V_R}$ with Fourier components proportional to $I_V(\omega)$.

With the TF coils inserted, $I_V(t)$ generates a magnetic field $\vec{B}_V(\vec{r}, t)$ with the components $B_{V_R}(\vec{r}, t)$ and $B_{V_Z}(\vec{r}, t)$. Their Fourier components are no longer proportional to $I_V(\omega)$ and can be written as

$$B_{V_{R,Z}}(\vec{r},\omega) = f_{R,Z}(\vec{r}) \cdot I_V(\omega) \cdot g_{R,Z}(\vec{r},\omega) \cdot e^{j\varphi_{R,Z}(\vec{r},\omega)} \quad (25a)$$

or

$$B_{V_{R,Z}}(\vec{r},\omega) = B^0_{V_{R,Z}}(\vec{r},\omega) \cdot g_{R,Z}(\vec{r},\omega) \cdot e^{j\varphi_{R,Z}(\vec{r},\omega)} \,. \quad (25b)$$

Quantities that belong to the horizontal component B_{V_R} are denoted by the suffix R, those belonging to the vertical component B_{V_Z} by the suffix Z. The functions $g_{R,Z}$, $\varphi_{R,Z}$ and $B^0_{VR,Z}$ are real quantities. In the low-frequency limit $\omega = 0$ the vertical magnetic fields with and without the TF coils (or any other conductors nearby) are identical:

$$B_{V_{R,Z}}(\vec{r},0) = B^0_{V_{R,Z}}(\vec{r},0) \quad (26)$$

It follows from eq. 25 together with eq. 26 that

$$g_{R,Z}(\vec{r},w) = |B_{V_{R,Z}}(\vec{r},w)| / |B_{V_{R,Z}}(\vec{r},0)| \tag{27a}$$

$$g_{R,Z}(\vec{r},0) = 1 \qquad \varphi_{R,Z}(\vec{r},0) = 0 \; . \tag{27b}$$

Four functions g_R, g_Z, φ_R and φ_Z have to be determined by measurements, while $I_V(w)$ can be computed for any current pulse $I_V(t)$ feeding the VF coils. The Fourier components of the resulting magnetic field $\vec{B}_V$ can be calculated with eq. 25 and the real-time magnetic field $\vec{B}_V(\vec{r},t)$ has to be computed by Fourier synthesis:

$$B_{V_{R,Z}}(\vec{r},t) = \frac{1}{2\pi} \cdot \int_{-\infty}^{+\infty} B_{V_{R,Z}}(\vec{r},w) \cdot e^{jwt} \, dw \tag{28}$$

The frequency dependence of $g_{R,Z}(\vec{r},w)$ and $\varphi_{R,Z}(\vec{r},w)$ was destined at six fixed frequencies by supplying the VF coils with sinusoidal currents of constant amplitude at the six frequencies selected. Forty-three measuring points (Fig. 3 a) across each of the two vertical cross-sections A-A and B-B (Fig. 3 b) were selected as lattice points in order to describe the space variables R, Z and the toroidal variable θ. The lattice points of the plane B-B are generated by turning the plane A-A 11.25 degrees around the Z-axis. Measurements were conducted at every lattice point for the six frequencies. It is necessary for the computation of the Fourierintegrals of eq. 28 to interpolate the measuring points in the frequency space by polynomials.

$B_{V_R}(\vec{r},w)$ and $B_{V_Z}(\vec{r},w)$ were measured with two Hall probes which are adjusted normal to each other. The output voltages of both probes are temperature stabilized better than -0.13 %/°K, and the permanency of sensitivity of both probes was checked in the interesting ranges of frequency and magnetic field strength to be better than 1 %.

The two output voltages of the probes were measured with heterodyne lock-in

analyzers which were synchronized by a sinusoidal signal proportional to $I_V(w)$.

A schematic diagram of the measuring electronics is shown in Fig. 4. At the beginning of each measurement the driving current through each Hall probe is set to zero. In spite of the shielding and twisting of the probe feeds large noise signals appear at the inputs of the lock-in analyzers which are induced by the time varying magnetic field. It is possible to set these error voltages to zero with the compensation electronics of Fig. 4. After adjusting the input voltage of the lock-in analyzers to zero the driving current of the Hall probes is switched on and the real amplitude and the phase shift against $I_V(w)$ of the Hall voltages is measured. The detection limit of this method is 0.01 σ .

Besides the electrical measuring errors there exists another source of error caused by the incorrect geometrical adjustment of the probes. Since B_{V_Z} is much larger than B_{V_R} inside the vacuum vessel, even small deviations of the B_R probe from the horizontal direction causes severe measuring errors, especially in the region near the horizontal midplane. The main adjustment errors of the two probes and of the movable probe holder are shown in Fig. 5.

The two Hall probes are fixed crosswise at the top of a cylindrical rod of insulating material. This probe holder is movable along its axis and normally to the horizontal midplane of the model. Even if the probe holder is adjusted along the R axis as well as possible, there always exist small deviations from the real R axis.

The deviations of the two-dimensional coordinate system R, Z describing the measuring system from the real coordinate system R^x, Z^x of the electrical model can be described by the two parameters $\bar{\alpha}$ and Δx_1 . These two correction quantities are very small in our model, as is shown later, and can be neglected in computing the magnetic field distribution. But they have to be used in order to determine the correction angle $\Delta\gamma$ of the B_R probe[1].

---

[1] In principle, a third correction quantity has to be used for the probe holder, but it is negligible in all cases.

The adjustment error of the B_R probe is described by two angles $\Delta\varphi$ and $\Delta\gamma$, and that of the B_Z probe by $\Delta\vartheta$. Denoting all quantities in the electrical model with stars and those determined with the measuring system without stars, the following correction formulas for the $B^x_{V_Z}$ and $B^x_{V_R}$ components are valid:

$$B_{V_R} = B^*_{V_R} \cdot \cos\Delta\varphi \cdot \cos\Delta\gamma + B^*_{V_Z} \cdot \sin\Delta\varphi \approx B^*_{V_R} + B^*_{V_Z} \cdot \Delta\varphi \tag{29a}$$

$$B_{V_Z} = B^*_{V_Z} \cdot \cos\Delta\vartheta + B^*_{V_R} \cdot \cos\varepsilon \cdot \sin\Delta\vartheta \approx B^*_{V_Z} \tag{29b}$$

The angle ε need not be specified since $|B^*_{V_R}| \ll |B^*_{V_Z}|$ and all correction angles are small quantities.

Rearrangement of eq. 29 is possible with these assumptions:

$$|B^*_Z| = |B_Z| \qquad \varphi^*_Z = \varphi_Z \tag{30a}$$

$$|B^*_R| = \left[|B_R|^2 + (\Delta\varphi \cdot |B_Z|)^2 - 2|B_R| \cdot |B_Z| \Delta\varphi \cdot \cos(\varphi_R - \varphi_Z)\right]^{\frac{1}{2}} \tag{30b}$$

$$\varphi^*_R = \arctan\left[\frac{|B_R| \cdot \sin\varphi_R - \Delta\varphi \cdot |B_Z| \cdot \sin\varphi_Z}{|B_R| \cdot \cos\varphi_R - \Delta\varphi \cdot |B_Z| \cdot \cos\varphi_Z}\right] \tag{30c}$$

with $B_R = |B_R| \cdot e^{j\varphi_R}$; $B^*_R = |B^*_R| \cdot e^{j\varphi^*_R}$; $B^*_Z = |B^*_Z| \cdot e^{j\varphi^*_Z}$.

It is necessary to determine $\Delta\varphi$ in order to solve eq. 30 . This can be performed by using the measured B_{V_R} and B_{V_Z} components along the R direction at every 9 lattice points in the planes Z = 0 and Z = 2.5 cm.

The transformation relations between the two coordinate systems now have to be considered which are given by

$$z^* = \Delta x_1 - R^*_o \cdot \tan\bar{\alpha} + R \cdot \sin\bar{\alpha} + z \cdot \cos\bar{\alpha} \approx z + (R - R_o) \cdot \tan\bar{\alpha} + \Delta x_1 \tag{31a}$$

$$R^* = R \cdot \cos\bar{\alpha} - z \cdot \sin\bar{\alpha} \qquad \approx R \tag{31b}$$

where $R_o \approx R^x_o$.

We can write the relations between the real magnetic field components in the model $B^{x}_{V_{R,Z}}$ and the measured quantities $B_{V_{R,Z}}$:

$$
\begin{aligned}
B_R(R,0) &= B_R^x(R,z_1^x) + B_z^x(R,z_1^x)\cdot\Delta\varphi \\
B_R(R,z_0) &= B_R^x(R,z_2^x) + B_z^x(R,z_2^x)\cdot\Delta\varphi \\
B_z(R,0) &= B_z^x(R,z_1^x) \\
B_z(R,z_0) &= B_z^x(R,z_2^x)\,,
\end{aligned}
\tag{32}
$$

using the notations

$$
\begin{aligned}
z_1^x &= z_1^x(R,0) = (R-R_0)\cdot\tan\bar{\alpha} + \Delta x_1 \\
z_2^x &= z_2^x(R,z_0) = z_0 + (R-R_0)\cdot\tan\bar{\alpha} + \Delta x_1 \\
z_0 &= 2.5\ cm
\end{aligned}
\tag{33}
$$

Linearization of eq. 32 together with eq. 33 yields in the low-frequency limit $\omega = 0$ the following fast converging iteration method for $\Delta\varphi$, Δx_1, $\bar{\alpha}$ and $B_R^x(R, Z_2^x)$:

$$B_R^{x(0)}(R_K,z_0) = B_R(R_K,z_0) \tag{34a}$$

$$B_z^x(R_K,0)\cdot\Delta\varphi^{(n+1)} + B_R^{x(n)}(R_K,z_0)\cdot z_1^{x(n+1)}(R_K,0)/2.5 - B_R(R_K,0) = 0 \tag{34b}$$

$$B_R^{x(n+1)}(R_K,z_0)\left[1 + z_1^{x(n+1)}(R_K,0)/2.5\right] + B_z^x(R_K,z_0)\cdot\Delta\varphi^{(n+1)} - B_R(R_K,z_0) = 0 \tag{34c}$$

with $n = 0,1\ldots$

$K = 1\ldots 9.$

Each iteration step includes the solution of 9 equations 34b ($K = 1 \ldots 9$) with the three independent variables $\Delta\varphi$, Δx_1 and $\bar{\alpha}$ by Gaussian error minimization.

3.4. Results

The measuring technique described in Sec. 3 was first checked in the electrical model without the TF coils. The measured magnetic field components of this so-called "vacuum case" were compared with a reference magnetic field. This reference field was numerically computed with high accuracy by using the exact dimensions of the VF coils of the model. As an example the measured and calculated magnetic field components of the "vacuum field" at Z = 2.5 cm are compared in Fig. 6 without any correction of the measured values.

A considerable improvement of the concidence of the B_{V_R} values can be achieved, expecially at the outer region of the electrical model, by using the correction method of Sec. 3.

One gets the following correction terms for the "vacuum case" after 5 iteration steps:

$$\Delta\gamma = -0.027^\circ, \qquad \Delta x_1 = 0.226 \text{ cm}, \qquad \bar{\alpha} = 0.18^\circ.$$

The maximum deviation $|\Delta B_{V_R}|$ of the corrected B_{V_R} component from the calculated one is

$$|\Delta B_{V_R}| < 6 \times 10^{-2}\, G,$$

and the maximum relative error of B_{V_R} is

$$(|\Delta B_{V_R}| / B_{V_R})_{MAX} = 10\ \%.$$

The vertical component B_{V_Z} of the "vacuum field" shows a systematic error (Fig. 6) probably caused by the calibration of the probe or the other measuring equipment. We used the computed B_{V_Z} values of all lattice points across the vertical cross-section of the model (Fig. 3 a) to correct the calibration of the measuring channel for the B_{V_Z} probe by Gaussian error minimization.

The correction factor for the B_{V_Z} channel yields

$$K = 1.037$$

with a maximum deviation of B_{V_Z}

$$|\Delta B_{V_Z}| < 0.5\ \sigma$$

and a maximum relative error

$$|\Delta B_{V_Z}/B_{V_Z}| < 5\%.$$

The diffusion of the vertical magnetic field through the TF magnet was mainly investigated on a sector with 6 double coils[1], but control measurements on a complete torus were also mode.

Some uncorrected results measured across the plane A-A of a torus sector with 6 double coils are shown in Figs. 7 to 12. The amplitudes and phase shifts of the B_{V_R} component are represented in Figs. 9 to 12 as functions of the major radius R with the measuring frequency as a parameter at two different horizontal planes Z = 2.5 cm and Z = 7.5 cm. The amplitudes of the corresponding B_{V_Z} component are shown in Figs. 7 and 8, while the phase shift φ_z of B_{V_Z} was measured to be nearly zero.

With 6 double coils inserted into the model of the TF magnet, its support structure

---

1) Very small differences (< 8 %) exist between the results for a complete torus and a sector with 6 double coils. All principle problems of the B_V diffusion through the TF magnet can therefore be investigated on such a sector.

is deformed somewhat, as can be seen from the correction terms.

$$\Delta\varphi = 0.27^{\circ}, \qquad \Delta x_1 = 0.23\ , \qquad \alpha = 0.31^{\circ},$$

which are somewhat changed compared with those without TF coils. These correction terms are used for calculating the time behaviour of the B_V field during adiabatic compression of the ZEPHYR plasma. The results of these calculations are shown in Sec. V.

4. Numerical calculation

The electromagnetic processes occurring on penetration of an electrically conducting wall by a time varying magnetic field is described by the diffusion equation

$$\Delta\vec{B} = \mu \cdot \varkappa \frac{\partial \vec{B}}{\partial t} \tag{35}$$

where $\vec{B}$ is the vector of the magnetic flux density, μ the permeability, and $\varkappa$ the electrical conductivity. For general geometries of the conducting wall this partial differential equation with given boundary and initial conditions cannot be solved analytically and can only be solved numerically with considerable effort /9./ . The approximation method presented in /7, 8/ is therefore used here.

4.1 Finite element network (FEN) method

In this method the electrically conducting wall is divided into finite elements from which an electrical network consisting of axial and transverse branches can be constructed. Assigned to each axial and transverse finite element is a network branch having an ohmic resistance R_μ , a self-inductance $L_{\mu\mu}$, and a mutual inductance $L_{\mu\nu}$ to all other branches of the network and the field-generating coils. The quanitties R_μ , $L_{\mu\mu}$ and $L_{\mu\nu}$ can be calculated from the geometry and position of the finite elements or coils. It is then possible to combine the network elements R_μ , $L_{\mu\mu}$, $L_{\mu\nu}$ of all network

branches in matrix form to yield a system of ordinary differential equations for the branch currents i_μ , $\mu = 1, 1, n$ as a function of time.

The distribution of the eddy currents in the wall and their time behaviour can be obtained direct from the branch currents. The final step is then to calculate the magnetic field of the eddy currents. By superposing the exciting field on this field for all times t, one obtaines the development of the diffusion process.

4.1.1 Representation of conducting wall as electrical network

A given, electrically conducting wall of thickness d is regarded here as being composed of finite elements. Serving as finite elements are two sets of rectangular plates superposed as in /7/, (Fig. 13 a). The plates aligned in the u-direction (u plates) carry the u-component of the eddy currents, and the plates aligned orthogonally to the others in the v-direction (v-plates) carry the v-component. With the plates arranged as in /7/ the centre lines of all the plates form a mesh network in which the u-plates are the axial branches, and the v-plates the transverse branches (Fig. 13 a). The approximation method presented in /7/ was derived for thin walls ($d \rightarrow 0$). It is now attempted here to extend the method to certain thick-walled structures. For this purpose n_w of the networks just described have to be placed on top of one another and their respective nodes also have to be connected with network branches in the w-direction (w plates), i.e. the thickness d of the conducting wall is divided into n_w layers, each having the thickness d_p. This yields a three-dimensional network which has n_u nodal planes in the u-direction, n_v in the v-direction, and n_w in the w-direction (Fig. 13) and has a total of

$$n = n_u (n_v - 1) n_w + (n_u - 1) n_v n_w + n_u n_v (n_w - 1) \qquad (36)$$

network branches. It should be noted that curved walls are also allowed, the limiting curve of the wall then being approximated by a polygon.

As will be shown later, the approximation of thick-walled structures quickly leads to very large networks the numerical analysis of which taxes the storage space and computing speed of present-day computers to their limits. For the problem concerned here a restriction therefore has to be made. Consideration is confined to networks without connecting branches in the w-direction. Between the n_w layers of a network (Fig. 13 b) there are thus no electrically conducting connections, i.e. there is only inductive coupling between branches of the various layers. By means of the FEN method such networks primarily allow reasonable approximation of multi-layer walls (e.g. winding form of a coil). The same applies to thick-walled structures which are penetrated essentially by a normal component of the field.

4.1.2 Calculation of network parameters

From the finite elements of the electrical network in Sec. 5.1.1 we now calculate the characteristic parameters $L_{\mu\nu}$, R_μ of the $\mu, \nu = 1, 1, n$ network branches. First we calculate the inductances, which for $\mu = \nu$ are self-inductances and for $\mu \neq \nu$ mutual inductances. Let i_μ be the current in the μ-th network branch (plate) and $\phi_{\mu m}$ the magnetic flux which is produced by the current i_μ, and which permeates the surface F_m defined by the branches s_1 to s_4 (Fig. 14). It is also generally valid that

$$\vec{B} = \mathrm{rot}\,\vec{A} \quad (\vec{B} \text{ magnetic flux density, } \vec{A} \text{ vector potential}), \tag{37}$$

$$\phi = \int_F \vec{B} \cdot d\vec{F} \tag{38}$$

With the Stokes theorem it follows that

$$\phi_{\mu m} = \int_{F_m} \vec{B}_\mu \cdot d\vec{F} = \int_{F_m} \mathrm{rot}\,\vec{A}_\mu \cdot d\vec{F} = \oint \vec{A}_\mu \cdot d\vec{s} \tag{39}$$

The resulting loop integral can now be split into four line integrals:

$$\phi_{\mu m} = \int_{s_1} \vec{A}_\mu \cdot d\vec{s} + \int_{s_2} \vec{A}_\mu \cdot d\vec{s} + \int_{s_3} \vec{A}_\mu \cdot d\vec{s} + \int_{s_4} \vec{A}_\mu \cdot d\vec{s} \tag{40}$$

which extend over the branches belonging to the m-th mesh. The flux $\phi_{\mu m}$ through the mesh m can thus be regarded as being composed of four partial fluxes $\phi_{\mu\nu}$, $\nu = 1, 1, 4$ from which the inductances

$$L_{\mu\nu} = \frac{\phi_{\mu\nu}}{i_\mu} = \frac{1}{i_\mu} \int_{S_\nu} \vec{A}_\mu \cdot d\vec{S} \tag{41}$$

between the μ-th and ν-th network branches can be calculated for $\mu, \nu = 1, 1, n$. For rectangular plates of thickness d_p in which constant current density G prevails the vector potential

$$\vec{A}_{(P)} = \frac{\mu_0}{4\pi} \cdot \int_V \frac{\vec{G} \cdot dV}{|\vec{R}|} \tag{42}$$

can be given in closed, analytical form at any space point P. Choosing the coordinate system and notation according to Fig. 15, one obtains for $A_{(p)}$ the following relation /10/:

$$A_{x\,(P)} = -\frac{\mu_0 G_x}{4\pi} \left\{ \sum_{i=1}^{8} sgn\left[y_{(i)} z_{(i)} x_{(i)}\right] \left[z_i x_i \ln (R_i + y_i) + y_i x_i \ln (R_i + z_i) \right.\right.$$

$$+ y_i z_i \ln (R_i + x_i) - \frac{z_i^2}{2} \arctan\left(\frac{y_i R_i + y_i^2 + z_i^2}{z_i x_i}\right) \tag{43}$$

$$\left.\left. - \frac{y_i^2}{2} \arctan\left(\frac{z_i R_i + y_i^2 + z_i^2}{y_i x_i}\right) - \frac{x_i^2}{2} \arctan\left(\frac{y_i R_i + y_i^2 + x_i^2}{z_i x_i}\right) \right] \right\}$$

with

$$\begin{aligned} x_i &= x_{(P)} - x_{(i)} \\ y_i &= y_{(P)} - y_{(i)} \\ z_i &= z_{(P)} - z_{(i)} \\ R_i &= \sqrt{x_i^2 + y_i^2 + z_i^2} \end{aligned} \tag{44}$$

$$sgn(f) = \begin{cases} 1 & \text{for } f \geq 0 \\ -1 & \text{for } f < 0 \end{cases}$$

Because of the condition $\vec{G}$ = const. within the plates the choice of the plate thickness d_p over the number of layers n_w must be such that the skin effect can be ignored. The line integral over A(p) for calculating the inductances is numerically solved by Gaussian quadrature.

The calculation of the mutual inductances

$$M_{\mu\nu} \quad \text{for} \quad \begin{matrix} \mu = 1, 1, n \\ \nu = 1, 1, n_e \end{matrix}$$

between the n branches of the FEN and the n_e external circuits (Fig. 15) is similar. Then the ohmic resistances R_μ, $\mu = 1, 1, n$ in the n network branches are calculated. From the geometry of the plates (Fig. 15) one can determine

$$R_\mu = \frac{l_\mu}{\varkappa \cdot F_\mu} \tag{45}$$

direct.

4.1.3 Symmetry and boundary conditions

In the numerical treatment of field diffusion problems any symmetries present should be utilized. A distinction is made between two types of symmetry, the so-called s and e-mirrors (Fig. 16):

a) In the s-mirror the symmetry plane is tangential to the eddy current lines.
b) In the e-mirror the symmetry plane is normal to the eddy current lines.

Figure 16 illustrates that, when a current line is reflected from an s-mirror, its true image with respect to distribution and direction is preserved. In reflection from an e-mirror, however, the distribtution of the current line is preserved but its direction is reversed. These symmetry properties allow the eddy current calculations to be restricted to a symmetric section of the structure considered, e.g. the first quadrant in the plate shown in Fig. 16. But the interaction between the circuits of the individual quadrants ought not to be left out of account. In the FEN case this means that one has to add to the mutual inductance between branches 1 and 2 of the first quadrant the mutual inductances between branch 1 and branches 3, 4 and 5, which

are located symmetrically to branch 2 (Fig. 16). The same procedure is used in calculating the self-inductances. Simple addition of the inductances is therefore permissible because the induced voltage in the μ-the network branch is described by

$$u_i = \sum_{\nu=1}^{n} L_{\mu\nu}\, i'_\nu \qquad (46)$$

and the derivatives of the currents with respect to time, i'_ν, at symmetrically located points are equal. This addition has, of course, to be performed with the correct sign. The appropriate sum term is positive when the eddy current and branch alignments (alignment of u and v-plates) are the same, and negative when they are opposite (Fig. 16).

Corresponding to the s and e-mirrors, a distinction is made between s and e-boundaries of the structure, it being possible to form some of the boundaries from symmetry planes. In Fig. 16 it is shown how to perform the discretization of the wall at the boundary, described in Sec. 5.1.1. The u or v-plates parallel to the boundary abut on an s-boundary (see v-plate 6), while they are halved by an e-boundary (see v-plate 7). Plate normal to the boundary abut on an e-boundary (see u-plate 1) and approach an s-boundary to within half a plate length (see u-plate 2).

4.1.4 Transient analysis of network

Before analysis of the derived RL network the calculated inductances and ohmic resistances are put in matrix form. With n network branches one obtains two n-dimensional, square matrices (L) and (R), the latter being a diagonal matrix. In the L matrix, on the other hand, the diagonal elements are the self-inductances of the network branches, and the off-diagonal elements are the mutual inductances. By means of Kirchhoff's equations

$$(i) = (H)(i_m), \qquad (47)$$

$$(0) = (H)^T(u) \qquad (48)$$

one can then give the differential equation of the network direct:

$$(i'_m) = -(L_m)^{-1}(R_m)(i_m) - (L_m)^{-1}(H)^T(u_o) \qquad (49)$$

/12/. The notation is as follows:

(i)	n-dimensional vector of branch currents,
(i_m)	m-dimensional vector of mesh currents,
(i'_m)	m-dimensional vector of derivative of (i_m) with respect to time,
(u)	n-dimensional vector of branch voltages,
(u_o)	n-dimensional vector of source voltages,
(H)	n . m-dimensional incidence matrix,
$(H)^T$	m · n-dimensional transposed incidence matrix
$(L_m)=(H)^T(L)(H)$	m·m-dimensional mesh inductance matrix, (50)
$(R_m)=(H)^T(L)(H)$	m·m-dimensional mesh resistance matrix. (51)

For given initial values $(i_{m(0)})$ this system of ordinary differential equations can be uniquely solved. From the solution vector (i_m) of the system of differential equations one obtains with the first Kirchhoff equation the vector (i) of the branch currents and hence the distribution of the eddy currents in the structure and their time behaviour. Furthermore, one obtains from the vector (i) the magnetic energy stored at time t

$$W = \frac{1}{2}(i)^T(L)(i) \qquad (52)$$

and the dissipated power

$$P = (i)^T(R)(i) \qquad (53)$$

Attention is brought to the special case of exclusively inductive excitation of the network that is relevant in the context of field diffusion. This is the case when, for example, just one current variation i'_e is given in the external circuits. The source

voltage is then obtained from

$$(u_o) = (L_{bx})(\dot{i}_e') \tag{54}$$

with (L_{bx}) of the n · k-dimensional matrix of the inductive couplings to the k external circuits.

4.1.5 Calculation of the magnetic field

Now that the eddy current distribution in the wall is known at any time, and hence the current density in each u, v and w-plate as well, it remains to calculate the magnetic field of these currents. In Sec. 5.1.2 the vector potential $\vec{A}$ for a plane slab with rectangular cross-section is described. With this and

$$\vec{B} = rot\ \vec{A} \tag{55}$$

one can determine the magnetic flux density $\vec{B}$ of all currents in the u, v and w-plates /13/. By superposing these field components one obtains the eddy current field at any space point.

The first field calculations here should, however, be done approximately. For this purpose the total current flowing in a u, v or w-plate is regarded as a line current concentrated on the centre line of the plate. These, in turn, are the branch currents of the network which were calculated in Sec. 5.1.4. The field calculation of the line currents is made according to /14/. For space points which are several plate lengths away from the wall this calculation method is certainly exact enough.

By superposing for all times t the magnetic field produced by the currents in the external conductors on that of the eddy currents one obtains the time development of the diffusion process.

4.1.6 Computer program

By the FEN method it is possible according to /7/ to divide the numerical solution of the field diffusion problem into four subsidiary ones:

a) Calculation of the network matrices (L) and (R)
b) Calculation of the inductive couplings (L_{bx}) to the external circuits
c) Solution of the differential equation of the network
d) Calculation of the magnetic flux density of the eddy currents.

This division was retained in extending the code described in /7/ to eddy current calculations in thickwalled structures. This extension called for essential modification of the program, the new version of which is shown in Fig. 17. As computing time and storage space requirements for diffusion calculations for thick-walled structures will be high, blocks a) to d) were made separately callable. By means of control parameters the user can choose the entry and exit points. Operations a) to d) can, of course, also be performed in one computing run. The results obtained after each of the four steps are stored in permanent files (Fig. 18) and are thus available at any time for subsequent calculations. For example, the field calculation according to d) can be repeated for different input parameters without rerunning the calculations a) to c) if their input parameters remain unchanged.

Storage space is allocated by "variable dimensioning", i.e. the individual matrices are assigned exactly tailored storage lengths from a global vector. By relocation in the global vector vacated data fields are erased or released for new matrices. This technique allows optimum utilization of the limited storage space availabel.

4.2 Sample calculation

The toroidal coil configuration (TF coils) of the planned ZEPHYR tokamak is used here as a sample calculation. The coil system has N = 16 coils, each composed of two pancakes separated by an insulating layer. Dimensions and design specifications are

given in Fig. 1. During plasma compression these coils are penetrated by a time varying vertical field generated in coils coaxial with the z-axis (external circuits; see Fig. 19). The maximum variation of the vertical field current necessary for compression is

$$\frac{\Delta i_v}{\Delta t} = 465 \ KA/sec$$

so that eddy currents are produced in the windings of the TF coils when they are penetrated by the vertical field. Owing to the disturbing influences of the eddy current field, described in Sec. 1, it is necessary to investigate the distribution and time behaviour of these fields in detail. For this purpose the winding forms of the TF coils are divided into u and v-plates in the FEN manner, there being per half pancake n_u divisions in the u-direction, n_v in the v-direction and n_w in the w-direction (Fig. 19 - 22). The pancakes are all delimited by s-boundaries (Fig. 19). In Fig. 19 - 22 only the u-plates are drawn because they fix the v-plates in any case, and so the figure is clear. The centre lines of all the plates form a network in which every branch corresponds to a u or v-plate. Taking the symmetries present into account, one can restrict analysis of the network to the subsidiary network of a half pancake, e.g. pancake half No. 16 in Fig. 20 for $z \geq 0$. One must, of course, calculate the inductances of all network branches and then combine them in each case into the resulting branch inductance of the subsidiary network.

In order to afford a simple possibility of comparision with measuring results, the diffusion process for sinusoidal excitation

$$i_v = i_o \sin \omega t \qquad (56)$$

of the V coils is investigated. First, however, it is shown by varying the number of branches n in the network that the numerical results converge towards a limiting value for increasing n. This is done with parameters n_u, n_v, n_w by succesively increasing one of them while keeping the other two constant. The computing runs a) to d) are performed for each version with the FEDIFF computer program. As the final result one obtains the magnetic field $B_{EC(t)}$ of the eddy currents at any point within the

torus. At the end of the transient ($t > 3\tau$) one can describe $B_{EC(t)}$ with a sinusoidal oscillation phase-shifted relative to the excitation:

$$B_{EC}(t) = B_0 \cdot \sin(\omega t + \varphi) \tag{57}$$

The amplitude B_z of the dominant component B_{ECz} is shown in Fig. 23 as a function of the divisions. The curves indicate that in all three cases converging solutions are obtained for an increasing number of branches in the network. A necessary condition is thus met by the code. The computing accuracies possible with the code are discussed in the following comparision with measuring results.

5. Discussion

The comparison of the measured and calculated magnetic fields was conducted for characteristic frequencies at special grid points on a sector of the tape-wound magnet of ZEPHYR consisting of 6 double coils (12 pancakes). The measured data were corrected by the method described in chapter 3.3. Because of a CPU time of nearly one hour for any job on an Amdahl computer only a few computed data could so far be obtained with the FEN code[1].

The comparison was therefore restricted to the plane A-A. Each pancake of the sector was approximated in toroidal direction by $n_u = 5$ and in poloidal direction by $n_v = 13$ conductor plates. In the radial direction $n_w = 3$ layers of conductor plates were used, each one insulated from the others.

---

[1] The CPU time will considerably be reduced, once the number of conducting plates is fixed for a given geometry.

Increasing deviations between measured and calculated magnetic field components can be expected for rising frequency especially for the magnetic field component in radial direction B_{V_R}.

Eddy current modes of high order will preferably be excited at high frequencies. And because of the finite number of conductor plates used for the approximation of a pancake, higher current modes cannot be computed by the FEN-code with the same accuracy as the ground mode. For the same reasons increasing deviations between measurements and calculations can be expected in the direct environment of the TF coils.

A comparison of the measured and computed B_{V_Z} components across the horizontal midplane for f = 200 Hz and for the highest frequency f = 1000 Hz to be considered for adiabatic compression of the plasma of ZEPHYR is represented in Fig. 24. Similar comparisons are shown in Fig. 25 across the horizontal plane at z = 0.25 m and in Fig. 26 at z = 0.5 m.

The maximum relative error between computed and measured B_{V_Z} values can be deduced from Figs. 24, 25 and 26 to be smaller than 5 % and is of the same order of magnitude as the measuring errors. No clear trend in the difference between measured and calculated B_{V_Z} values with frequency and with distance between grid points and conducting materials can therefore be derived from these results.

A phase shift of nearly zero between B_{V_Z} and the current through the VF coils was measured and calculated at any grid point and indicates a predominance of the ground mode (saddle currents) in changing the B_{V_Z} component.

The behaviour of the B_{V_R} component across the horizontal planes at z = 0.25 m and z = 0.5 m is represented in Figs. 27 and 28. It should be kept in mind that the B_{V_R} component only amounts to one-tenth of the vertical field component B_{V_Z}. It is surprising that not only do the measured and calculated amplitudes of B_{V_R} agree well

but also the measured and calculated phase shifts between B_{V_R} and the current through the VF coils coincide better than 5 %. Small deviations from the current phase shifts critically influence the real-time response of the B_{V_R} component to a current pulse through the VF coils, while the influence of amplitude errors on the result is much smaller.

This especially good agreement between the measured and calculated phase shifts of B_{V_R} allows sufficiently accurate computation of the real-time behaviour of B_{V_R} during adiabatic compression or during feedback stabilization with the FEN code. The vertical and radial plasma positions can be calculated at any moment together with the current shape of the plasma flux surfaces if one uses an appropriate equilibrium code coupled with the FEN code.

In any case the FEN code allows computation of poloidal field distortions and of the electromagnetic forces acting on the TF coils or other conducting structures.

References:

/1/ "Compact Ignition Experiment", Status Report prepared by IPP Garching and CNEN Frascati, September 1978

/2/ D.B.Albert, H.Winter, Report IPP III/58, February 1980

/3/ "Toroidal Field Magnet for ZEPHYR", Status Report June 1980

/4/ H.Kotzlowski, K.F.Mast, H.Preis, Report IPP I/175, November 1979

/5/ Private communication, B.Streibl

/6/ K.F.Mast, "Electric Model of the Vacuum Vessel of ZEPHYR", Report IPP I/174, November 1979

/7/ U.R.Christensen, "Time Varying Eddy Currents on a Conducting Surface in 3-D using a Network Mesh Method", PPPL-1516, April 1979

/8/ D.W.Weissenburger, U.R.Christensen, "Transient Eddy Currents on Finite Plane and Toroidal Conducting Surfaces, PPPL-1517, April 1979

/9/ A.Kameari et al., "Eddy Currents Induced on a Resistive Shell with Cuts, JAERI-M-6468, 1976

/10/ S.J.Sackett, "EFFI-A Code for Calculating the Electromagnetic Field, Force, and Inductance in Coil Systems of Arbitrary Geometry, UCRL-52402, March 1978

/11/ H.Preis, F.Schneider, "Bestimmung von Wirbelströmen im Vakuumgefäß einer Apparatur zur Erforschung der kontrollierten Kernfusion, Archiv für Elektrotechnik 62 (1980), 181 - 186

/12/ H.Preis, "Die Analyse transienter Vorgänge in linearen, elektrischen Netzwerken, IPP-Report 4/87, 1971

/13/ L.R.Turner et al., "A Three-Dimensional Analytic Modell for Calculating Eddy-Current Effects Applied to a Tokamak Blanket and Shield, Proc. Compumag 1976

/14/ H.Preis, Calculation of the Magnetic Field, Magnetic Forces and Behaviour of Large Coil Systems for Fusion Experiments, IPP 3/24, 1976

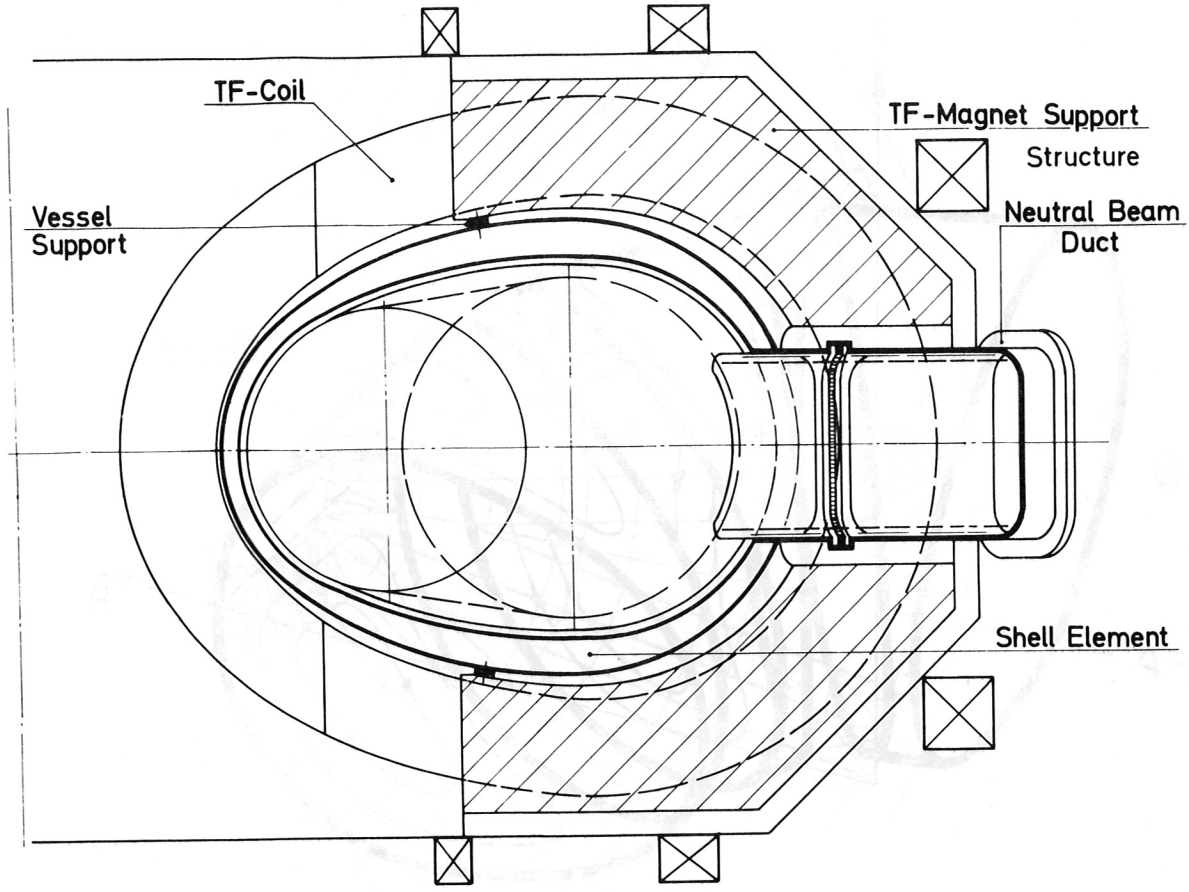

Fig. 1 a: Vertical section of ZEPHYR.

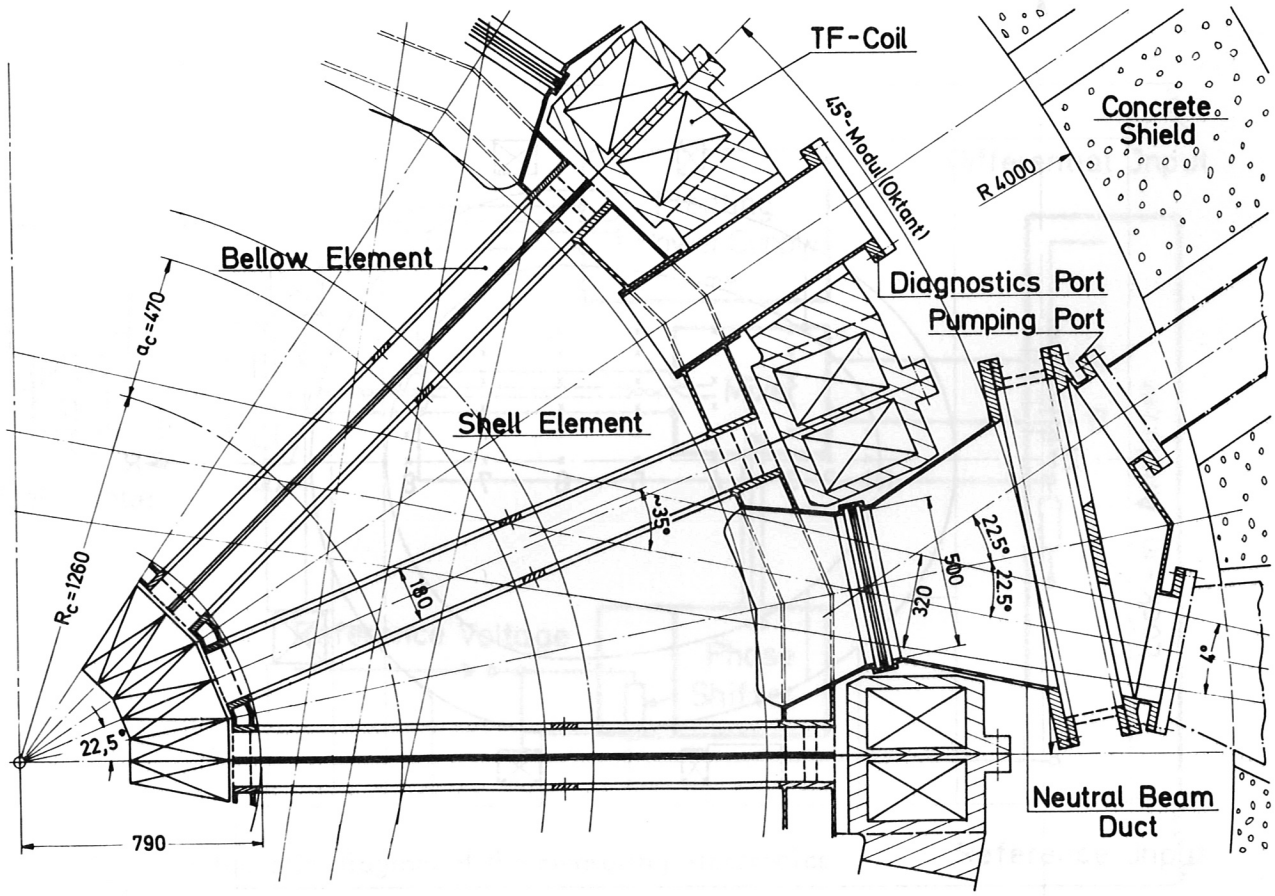

Fig. 1 b: Equatorial section of ZEPHYR.

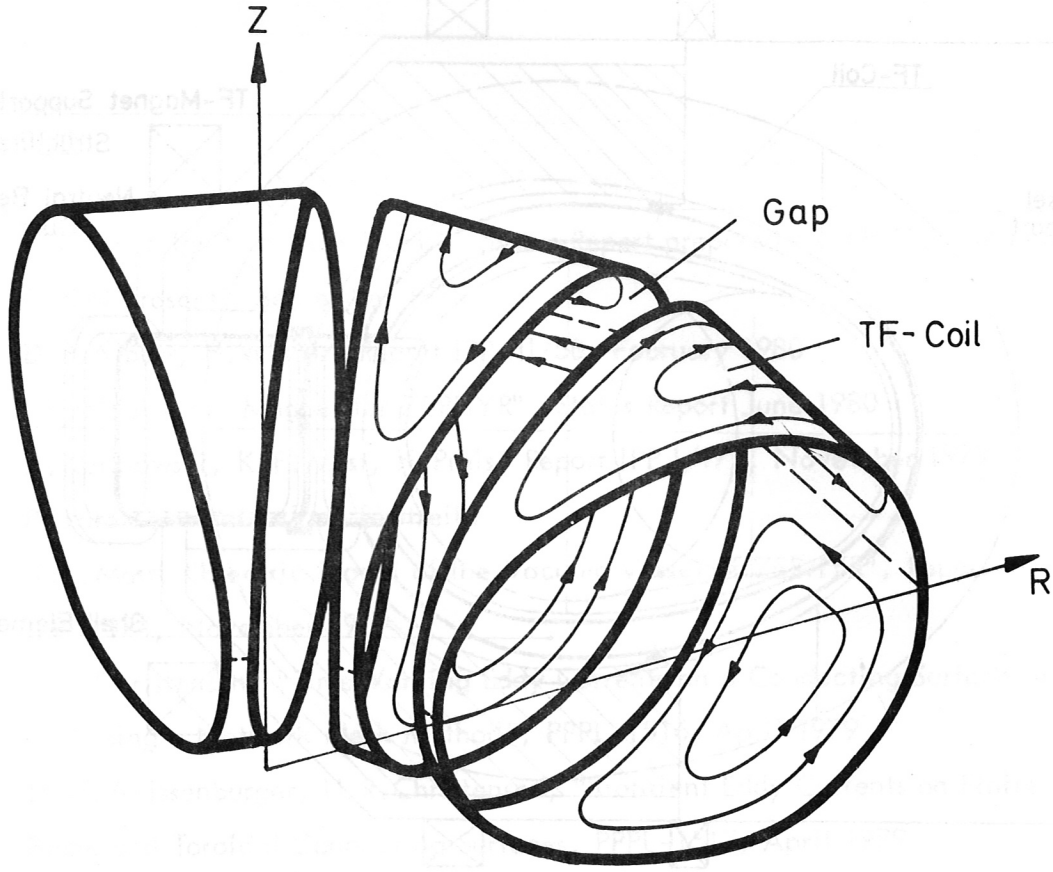

Fig. 2: Schematic representation of the saddle currents on the TF coils.

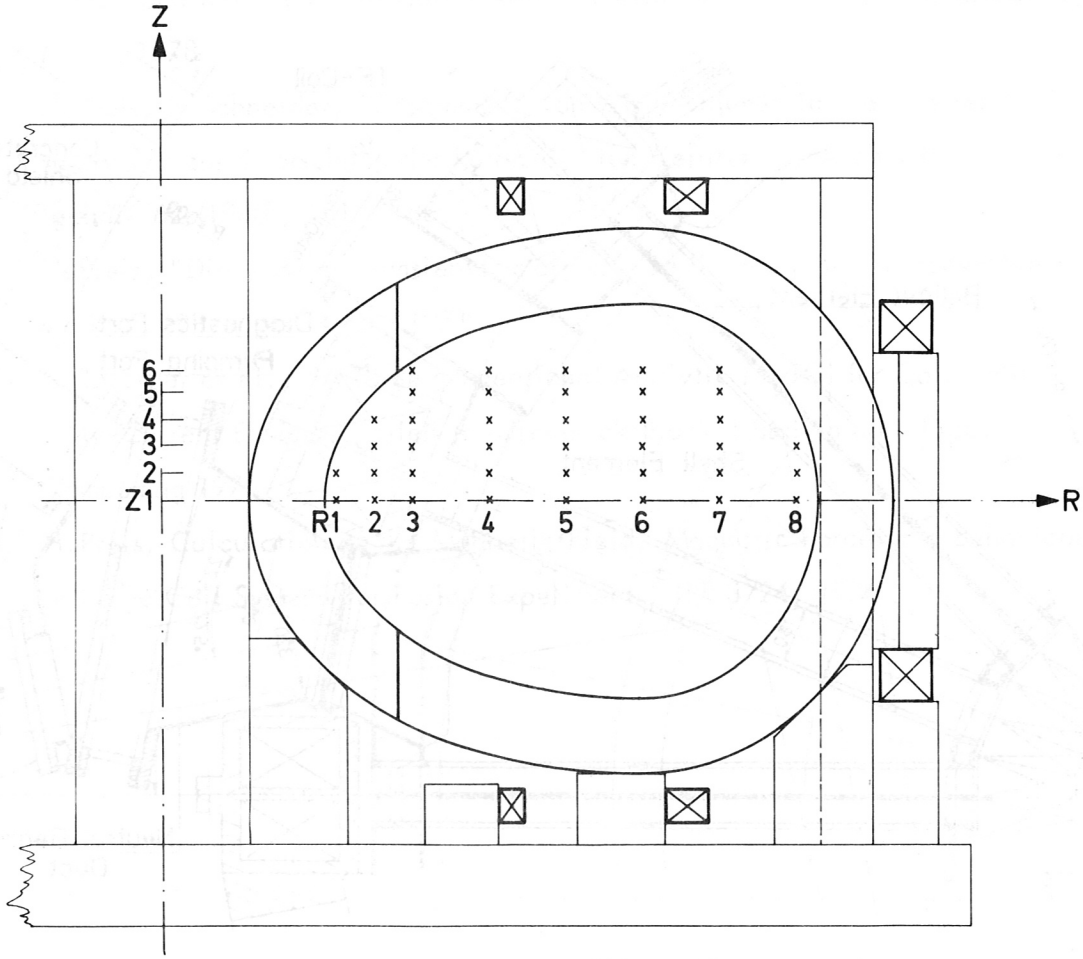

Fig. 3 a: Vertical section of the electrical model.

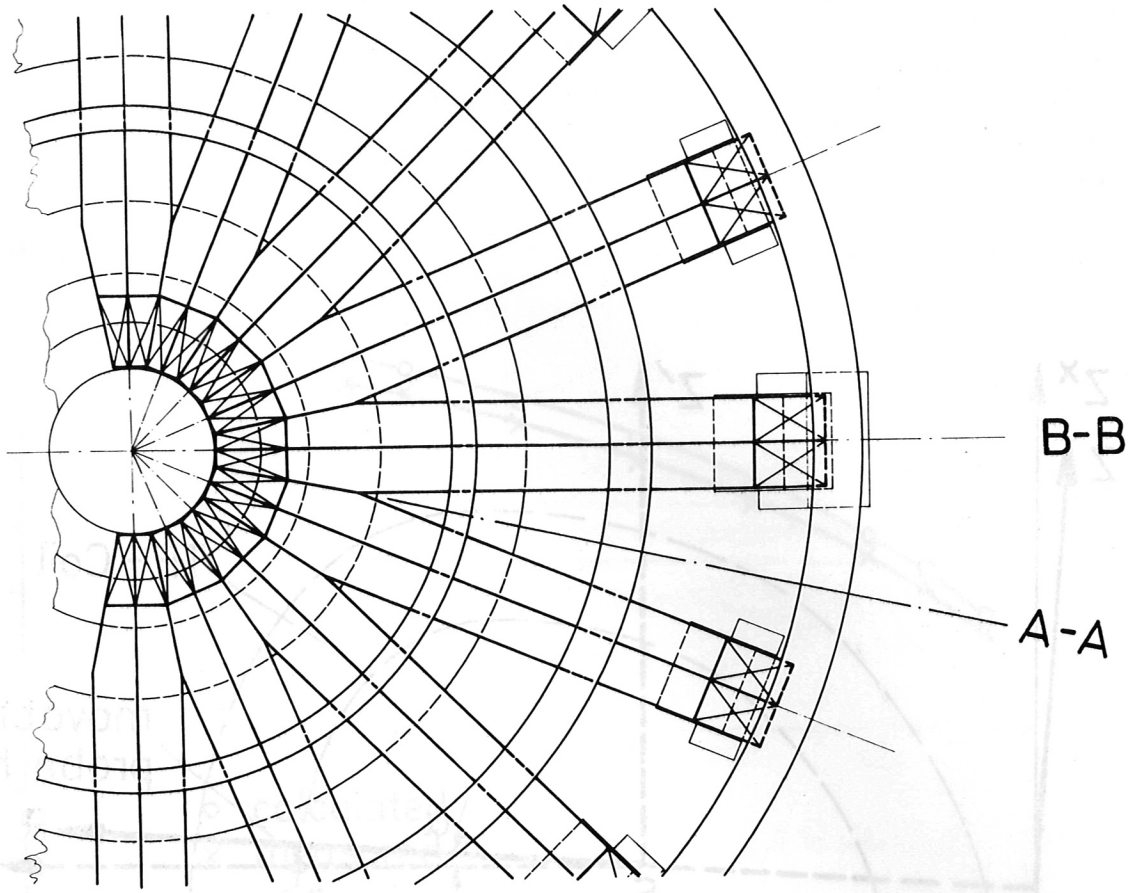

Fig. 3 b: Equatorial section of the electrical model.

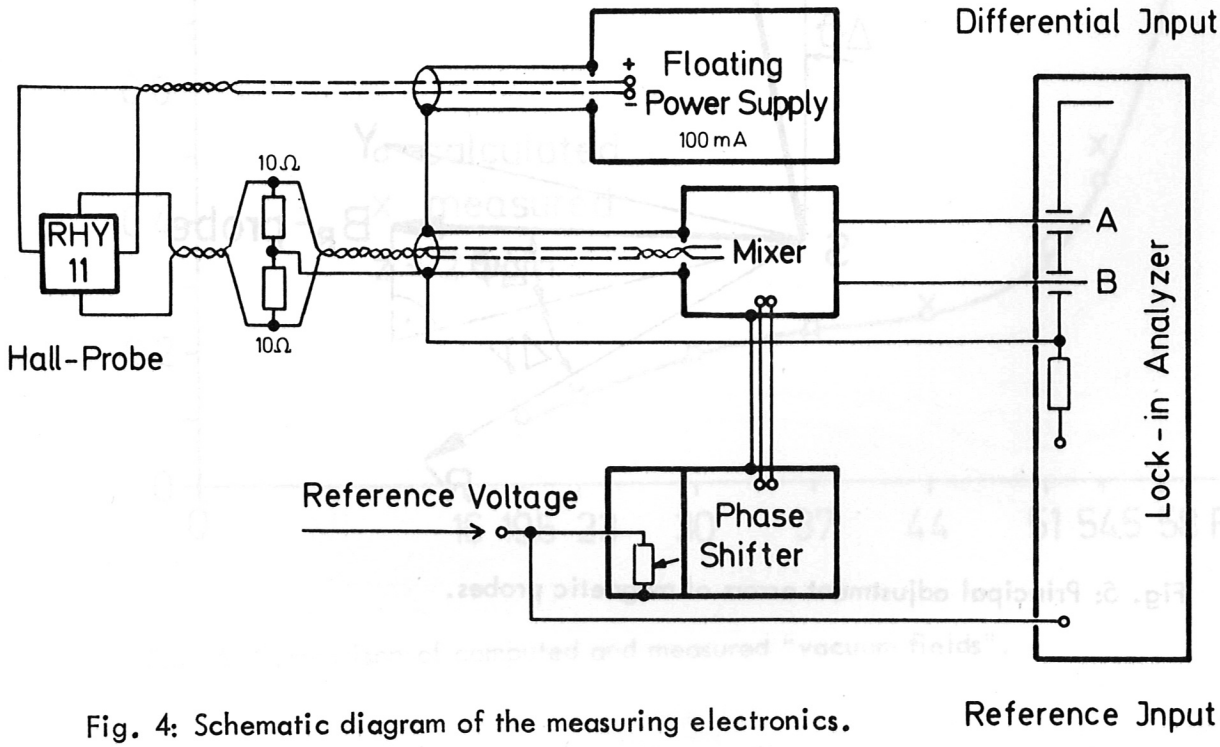

Fig. 4: Schematic diagram of the measuring electronics.

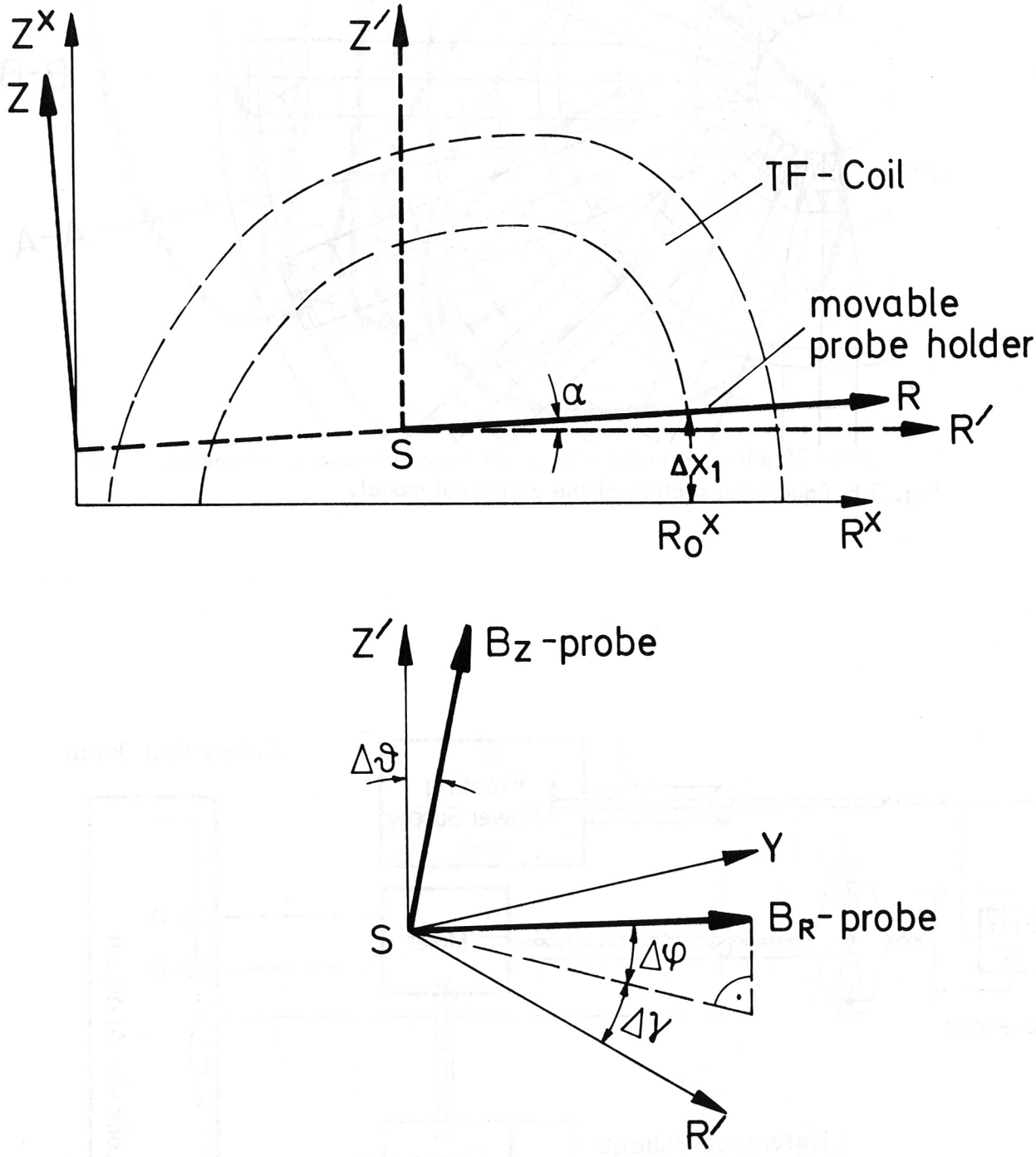

Fig. 5: Principal adjustment errors of magnetic probes.

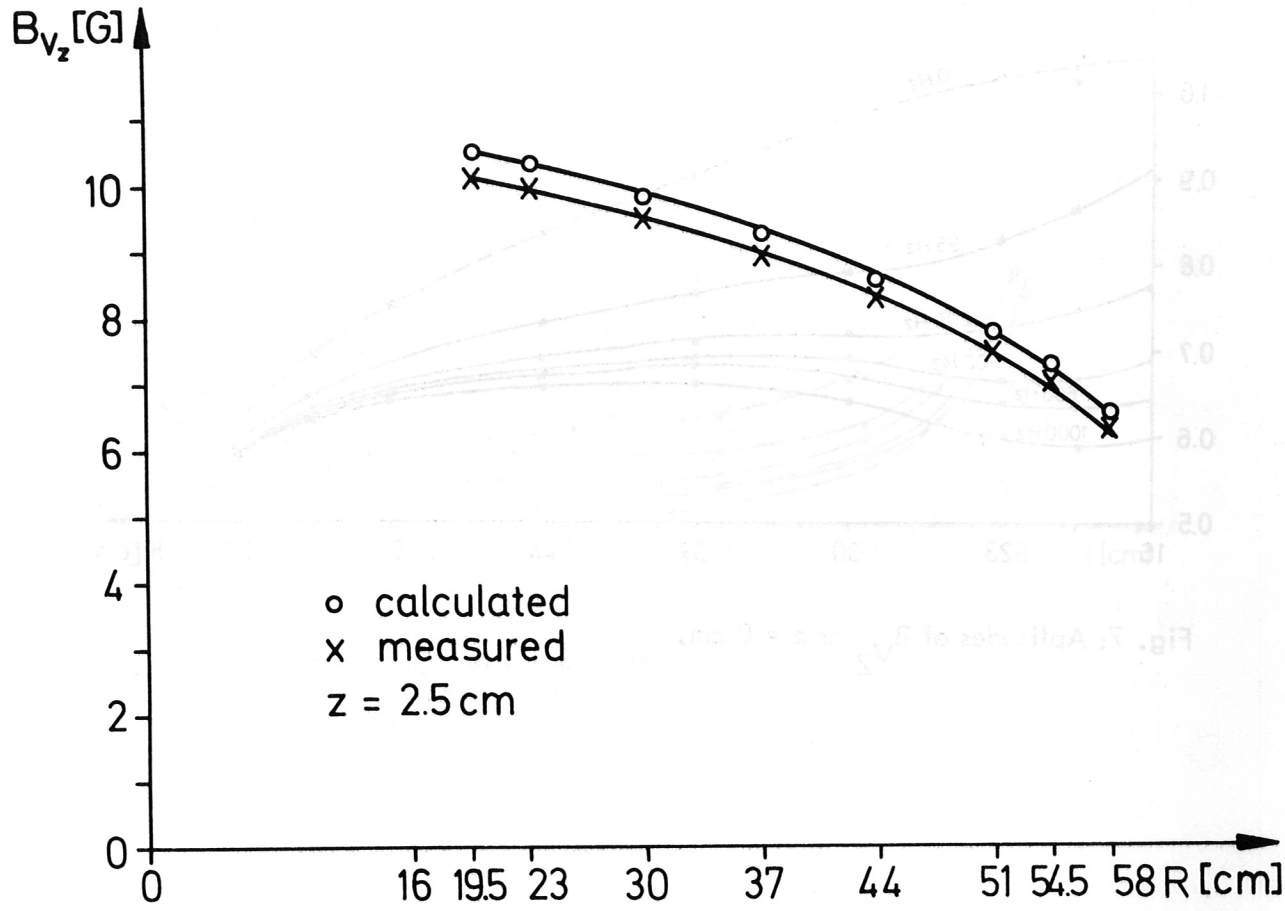

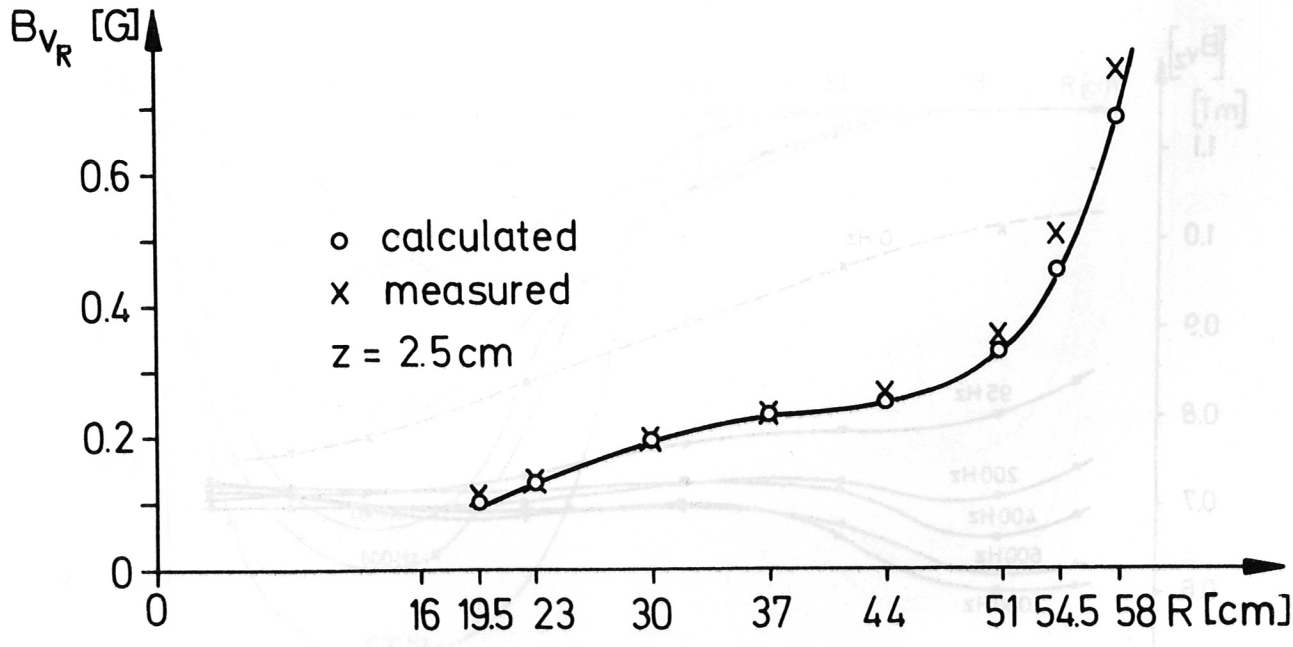

Fig. 6: Comparison of computed and measured "vacuum fields".

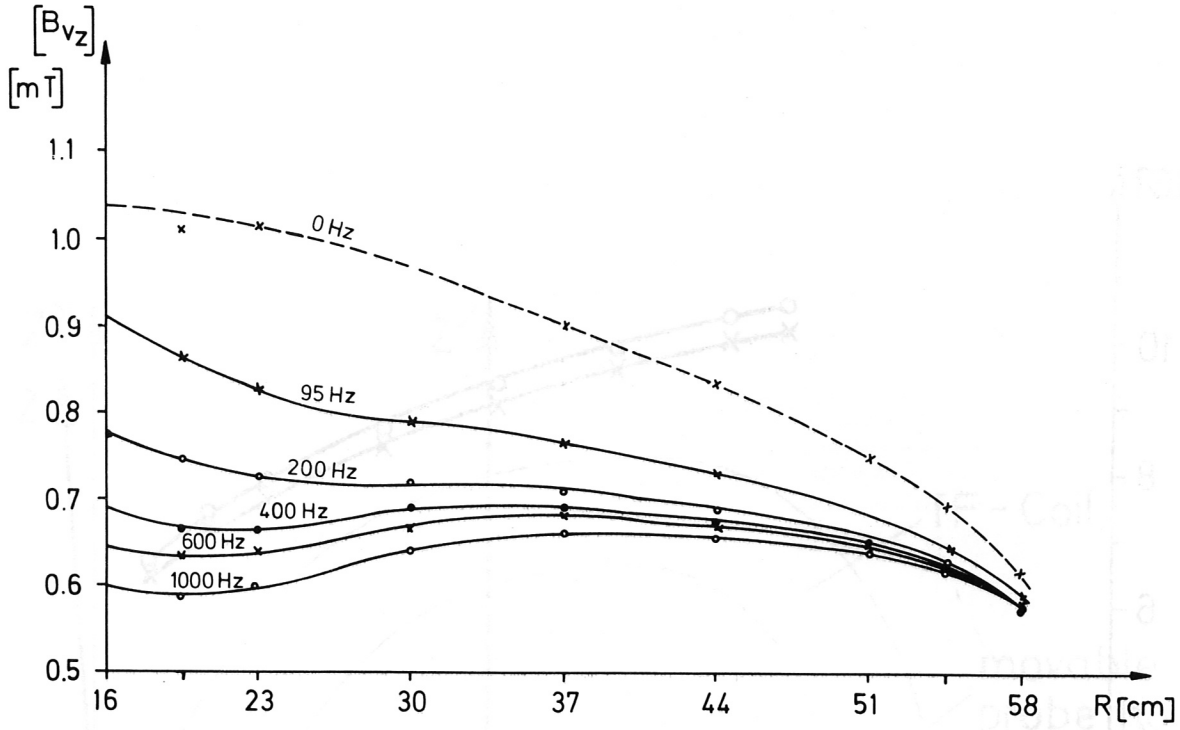

Fig. 7: Aplitudes of B_{VZ} at z = 0 cm.

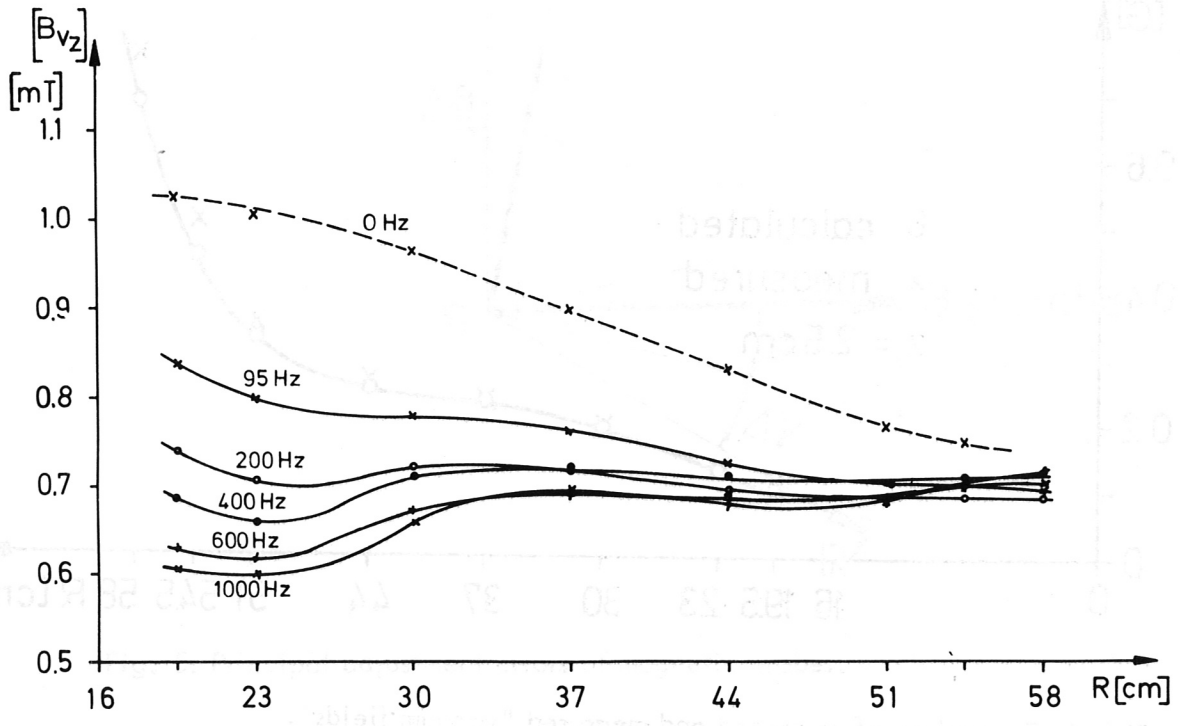

Fig. 8: Amplitudes of B_{VZ} at z = 7.5 cm.

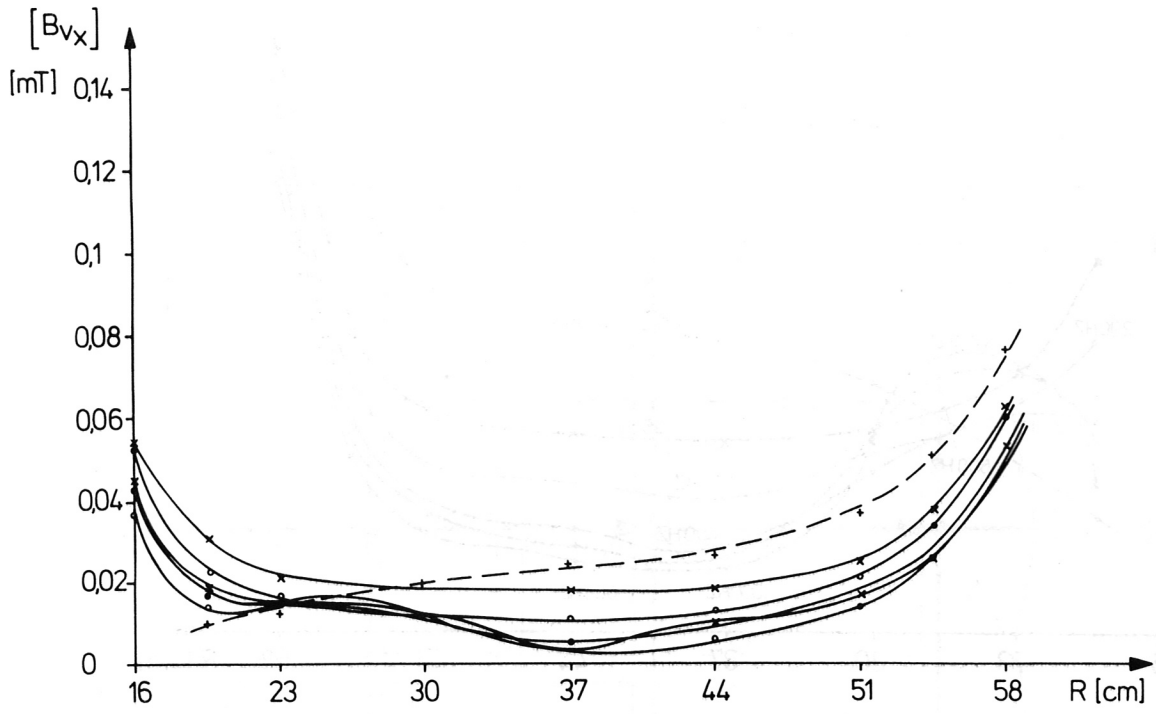

Fig. 9: Amplitudes of B_{V_R} at z = 2.5 cm.

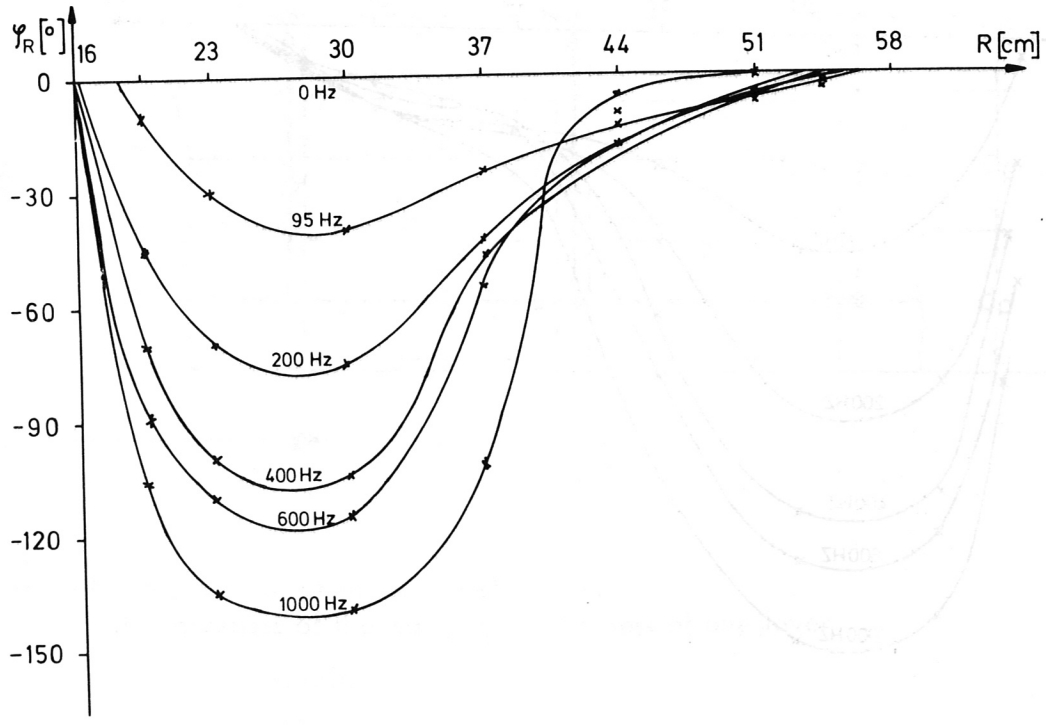

Fig. 10: Phase shifts of B_{V_R} at z = 2.5 cm.

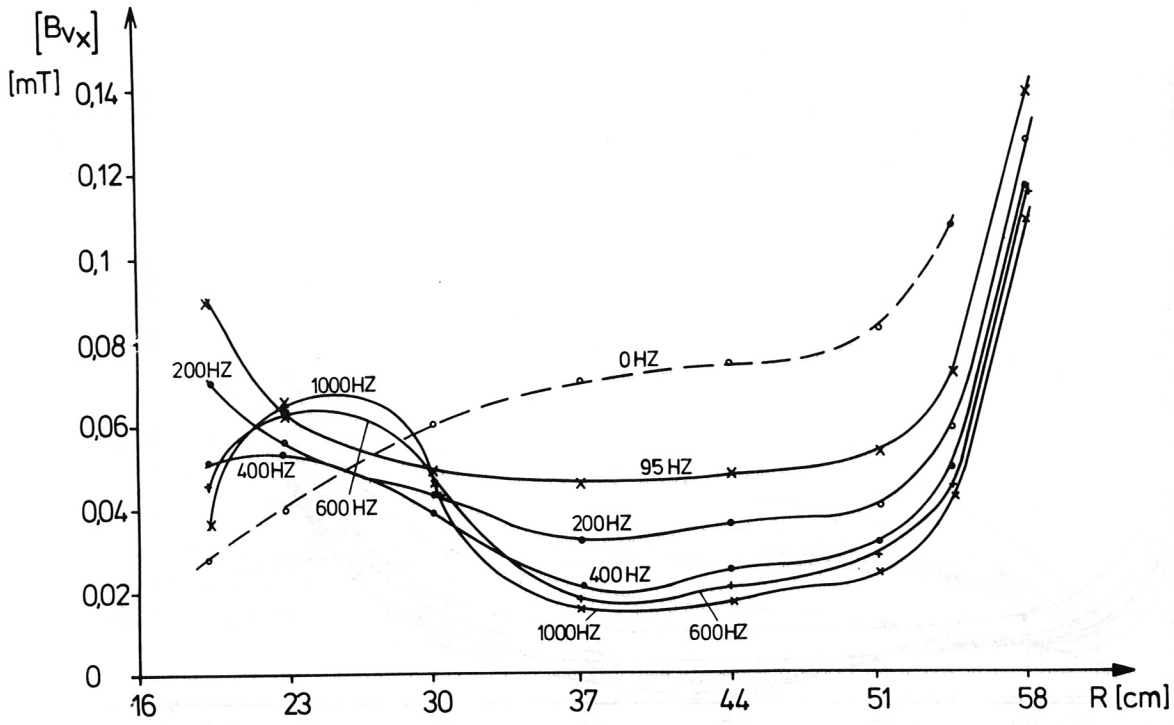

Fig. 11: Amplitudes of B_{V_R} at z = 7.5 cm.

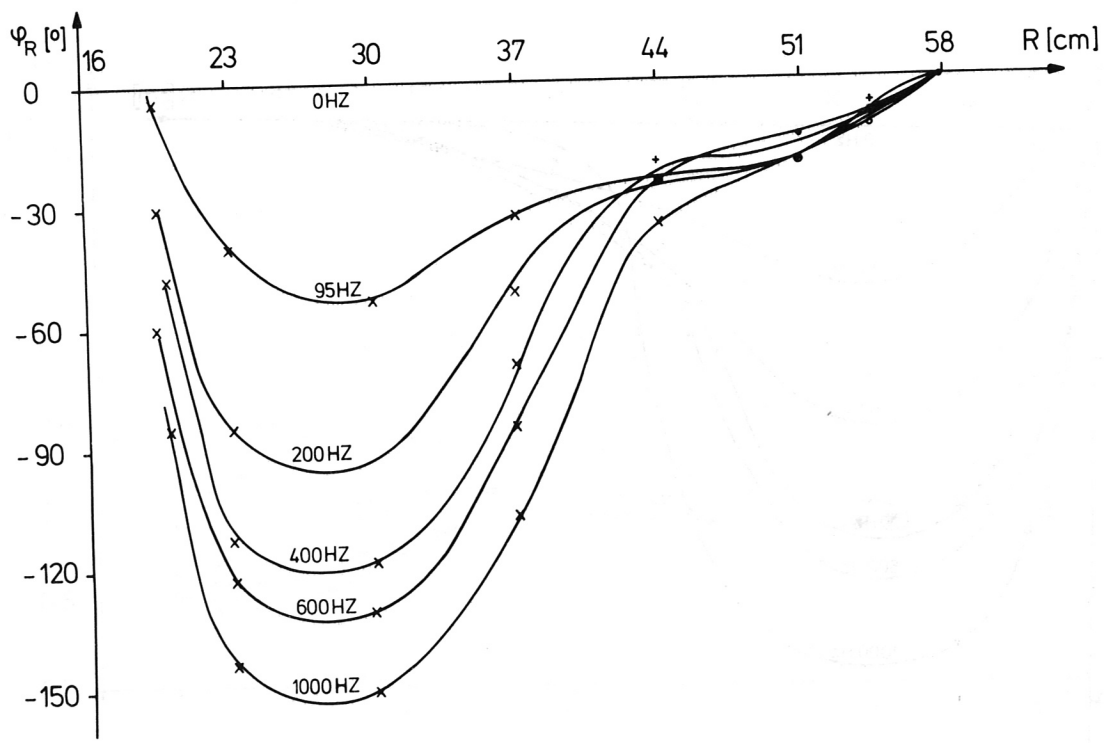

Fig. 12: Phase shifts of B_{V_R} at z = 7.5 cm.

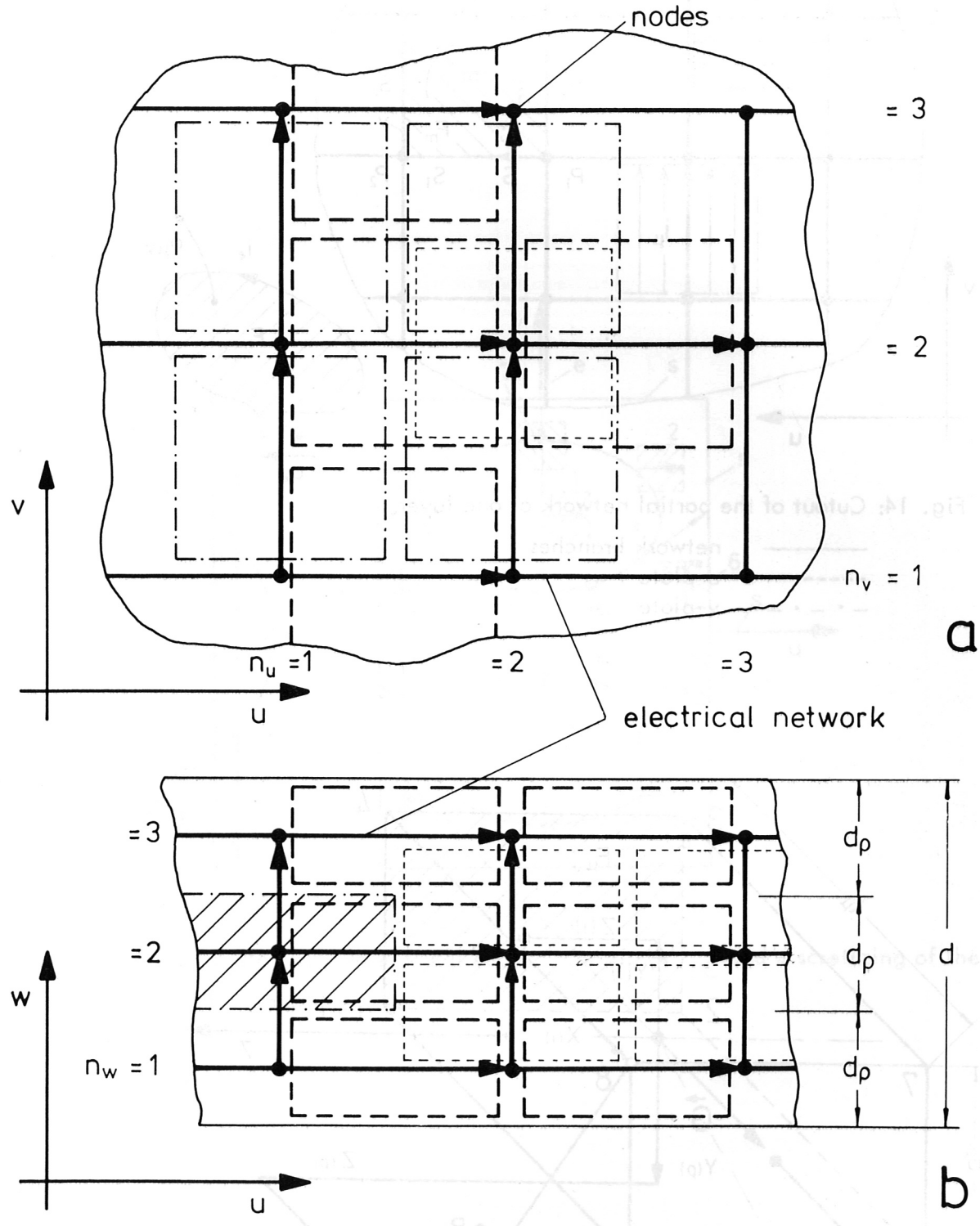

Fig. 13: Arrangement of the finite elements.
d thickness of the wall, d_p thickness of one layer

- - - - - u-plate
— · — · — v-plate
..... w-plate

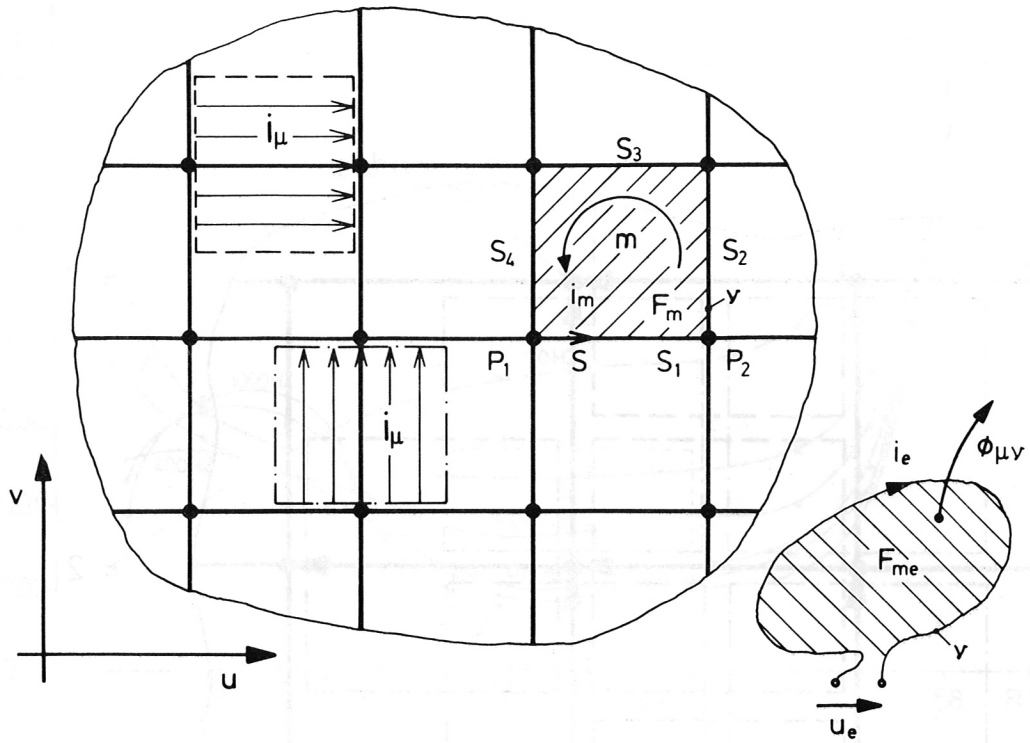

Fig. 14: Cutout of the partial network of one layer.

——— network branches
- - - - - - - - u-plate
– · – · – v-plate

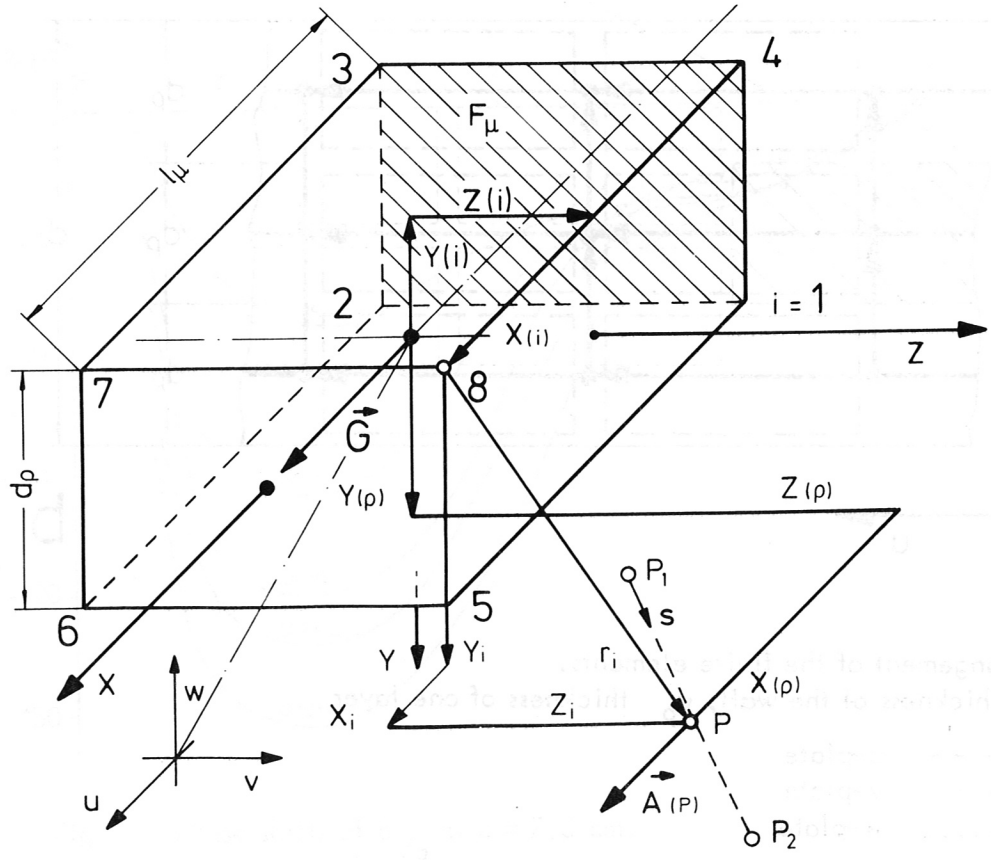

Fig. 15: Decription of the vector potential of a spacial conductor.

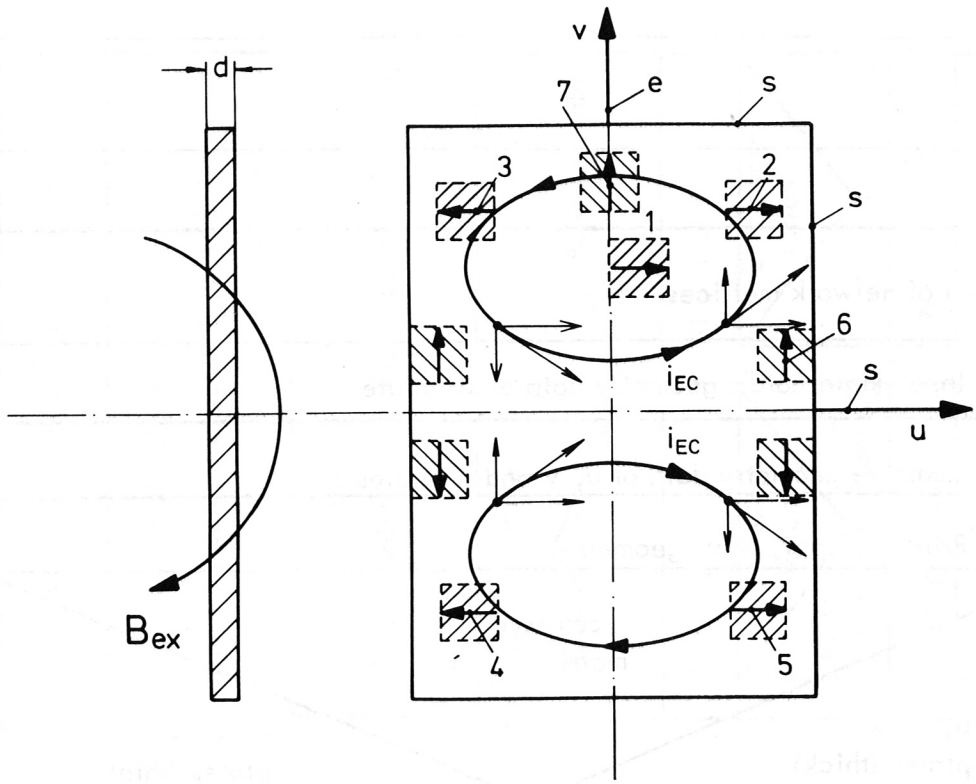

Fig. 16: Plane plate with symmetrical eddy current lines i_{EC} and discretizing of the plate by u and v-plates.

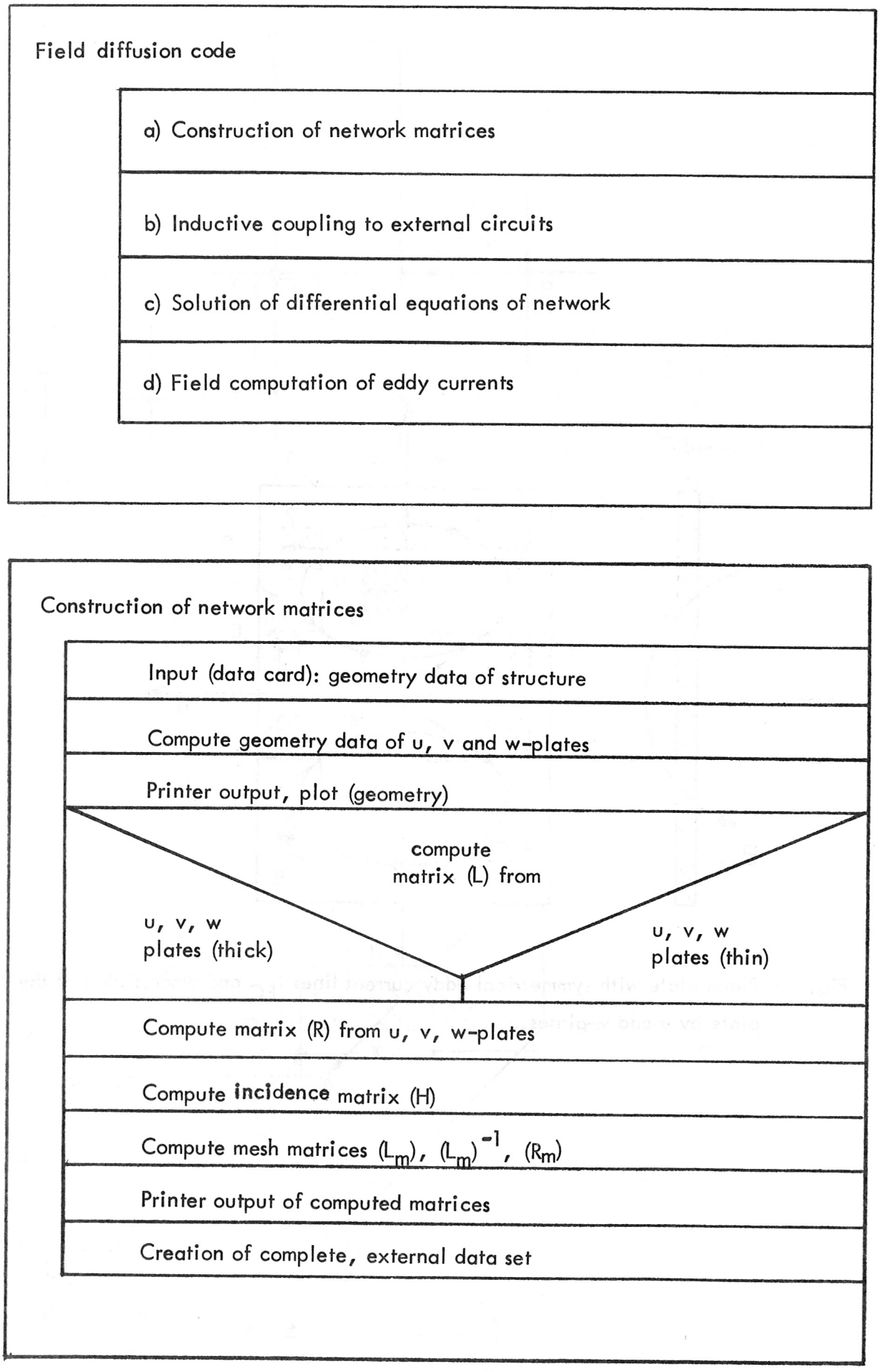

Fig. 17: Structogram of field diffusion code, Part 1.

b)

Inductive coupling to external circuits

Input (external data set):
Geometry data of u, v and w-plates

Input (data card):
data of external conductors

Computation of (L_{bx})

Creation of complete, external data set

c)

Solution of diff. equations of network

Input (external data set):
geometry data, matrices (R_m), (L_m), (L_{bx})

Input (data card):
data for solving differential equation

Solution method according to

Runge-Kutta

Bulirsch-Stöhr

$0 \leq t \leq t_e$

Ext. excitation

Num. funct.

Anal. funct.

Printer output

Output of ext. storages

$0 \leq t \leq t_e$

Ext. excitation

Printer output

Output of ext. storages

Creation of complete, external data set

d)

Field comp. of eddy currents

Input (external data set):
geometry data

Input (data card):
space point data, control data

$t_a \leq t \leq t_e$

Input (external data set):
currents (i)

For all u, v, w-plates

Conductor definition Field comp. of cond. Superposition

Printer output

Output of ext. storages

Creation of complete, external data set

Fig. 17: Structogram of field diffusion code, Part 2.

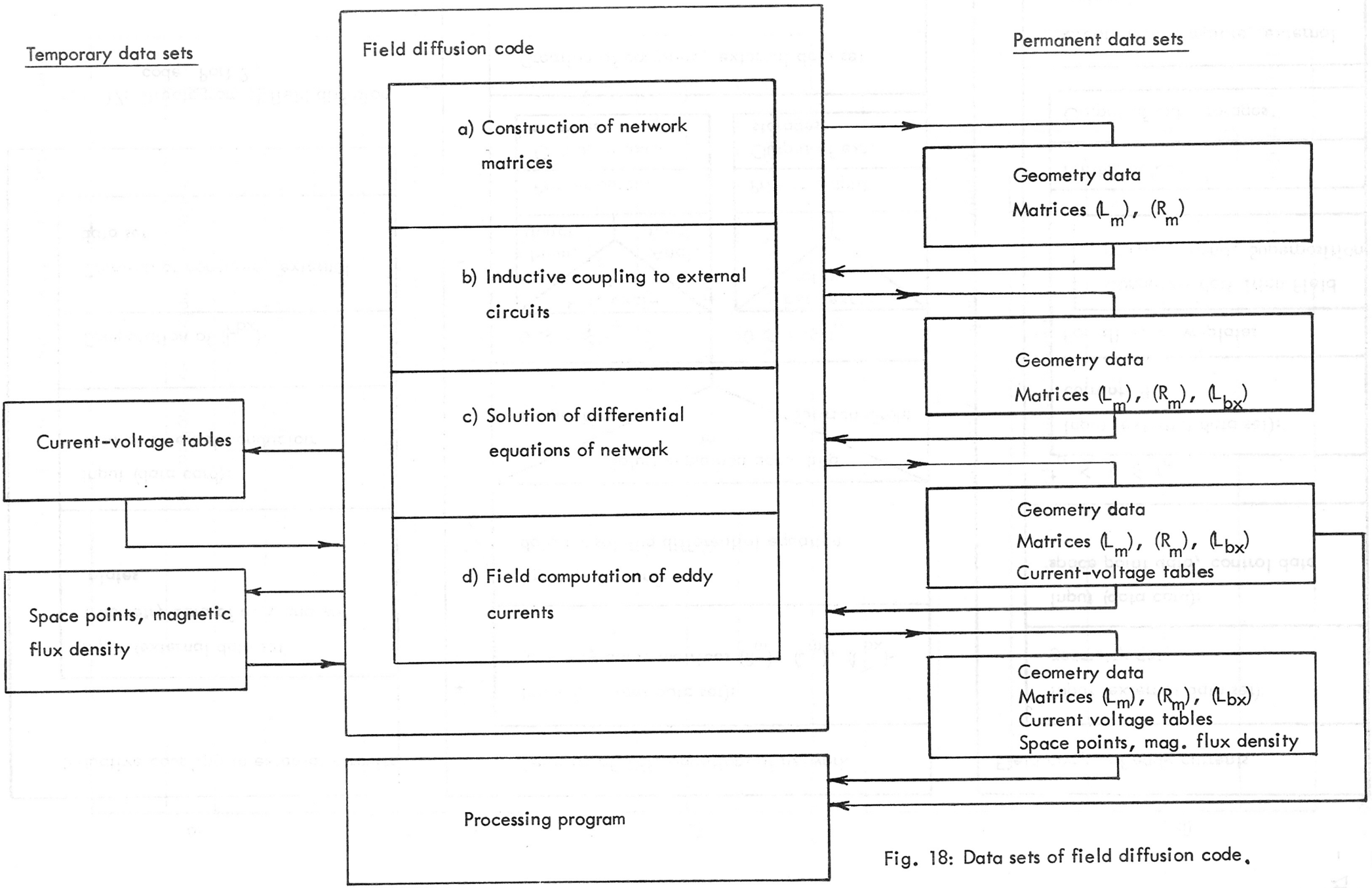

Fig. 18: Data sets of field diffusion code.

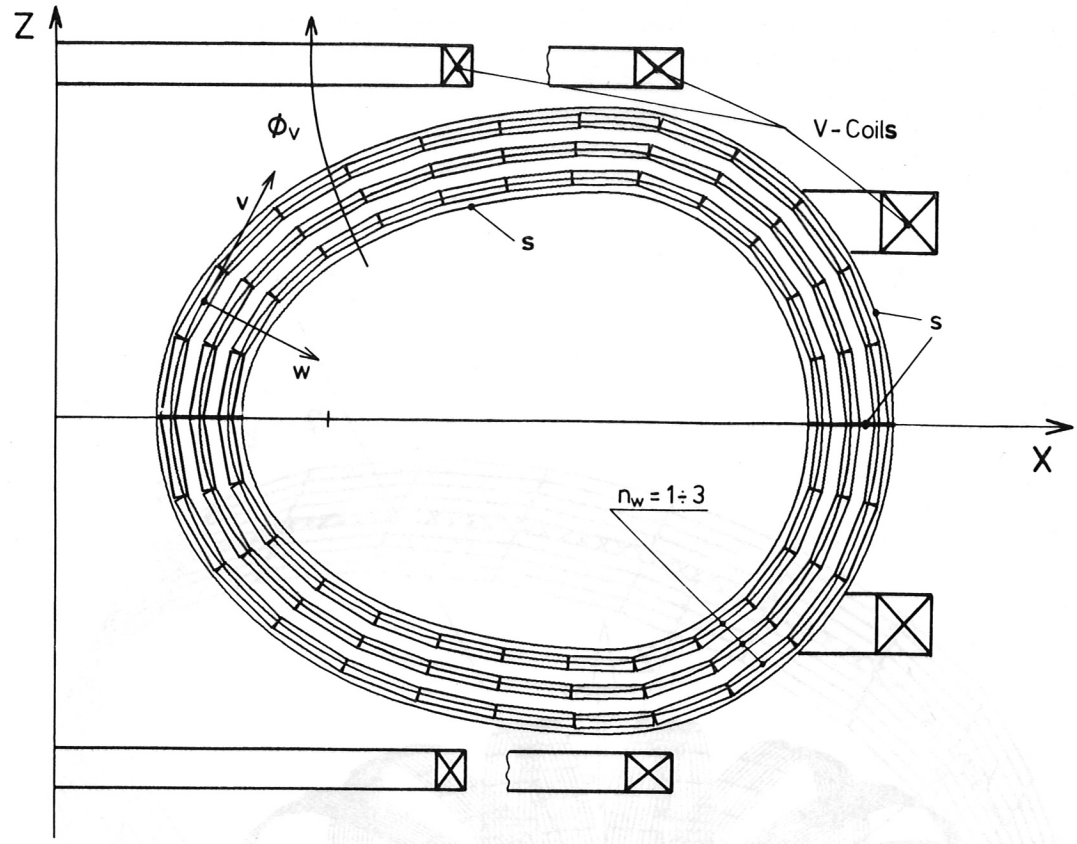

Fig. 19: Cross-section A-A (see Fig. 20) of the TF and V coils with distribution of the u-plates for $n_w = 3$.

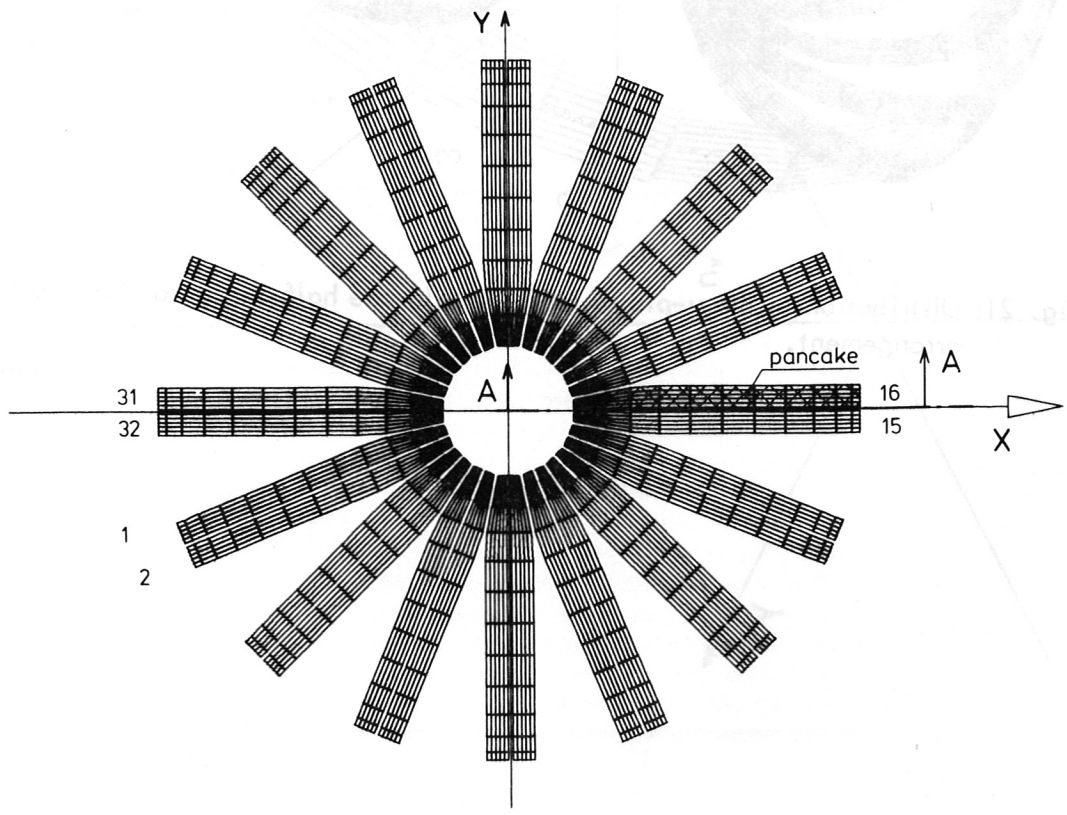

Fig. 20: Top view of the toroidal coil arrangement with distribution of the u-plates for $n_u = 5$, $n_v = 13$.

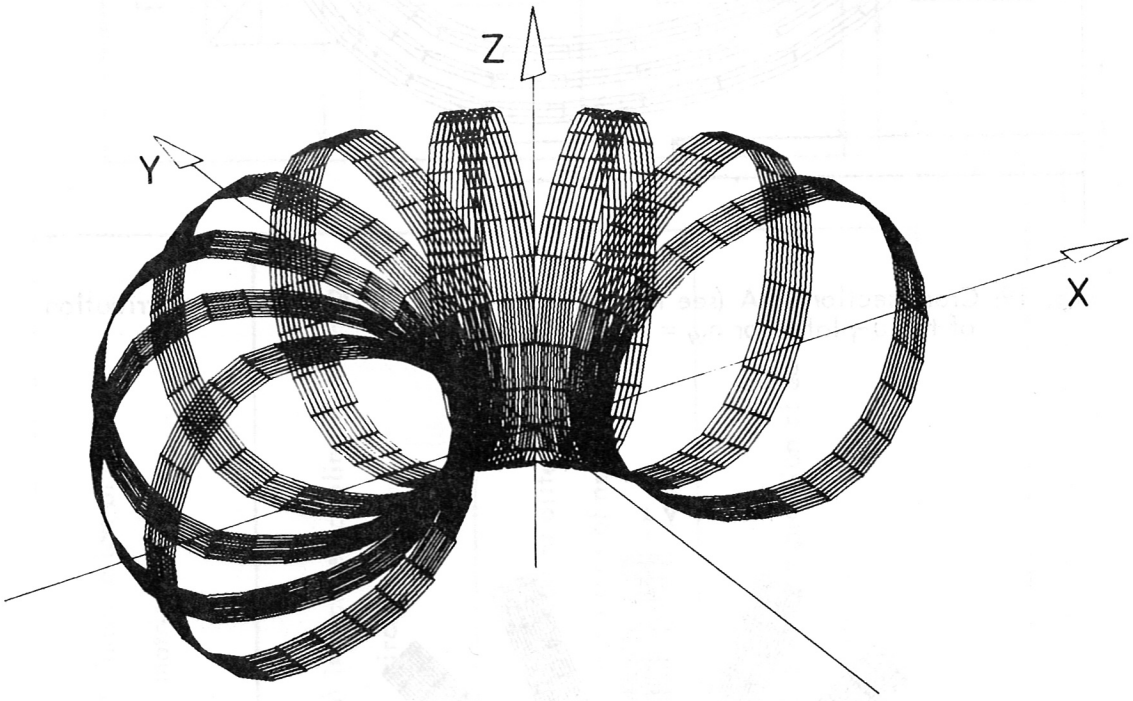

Fig. 21: Distribution of the u-plates for $n_w = 1$ in one half on the toroidal coil arrangement.

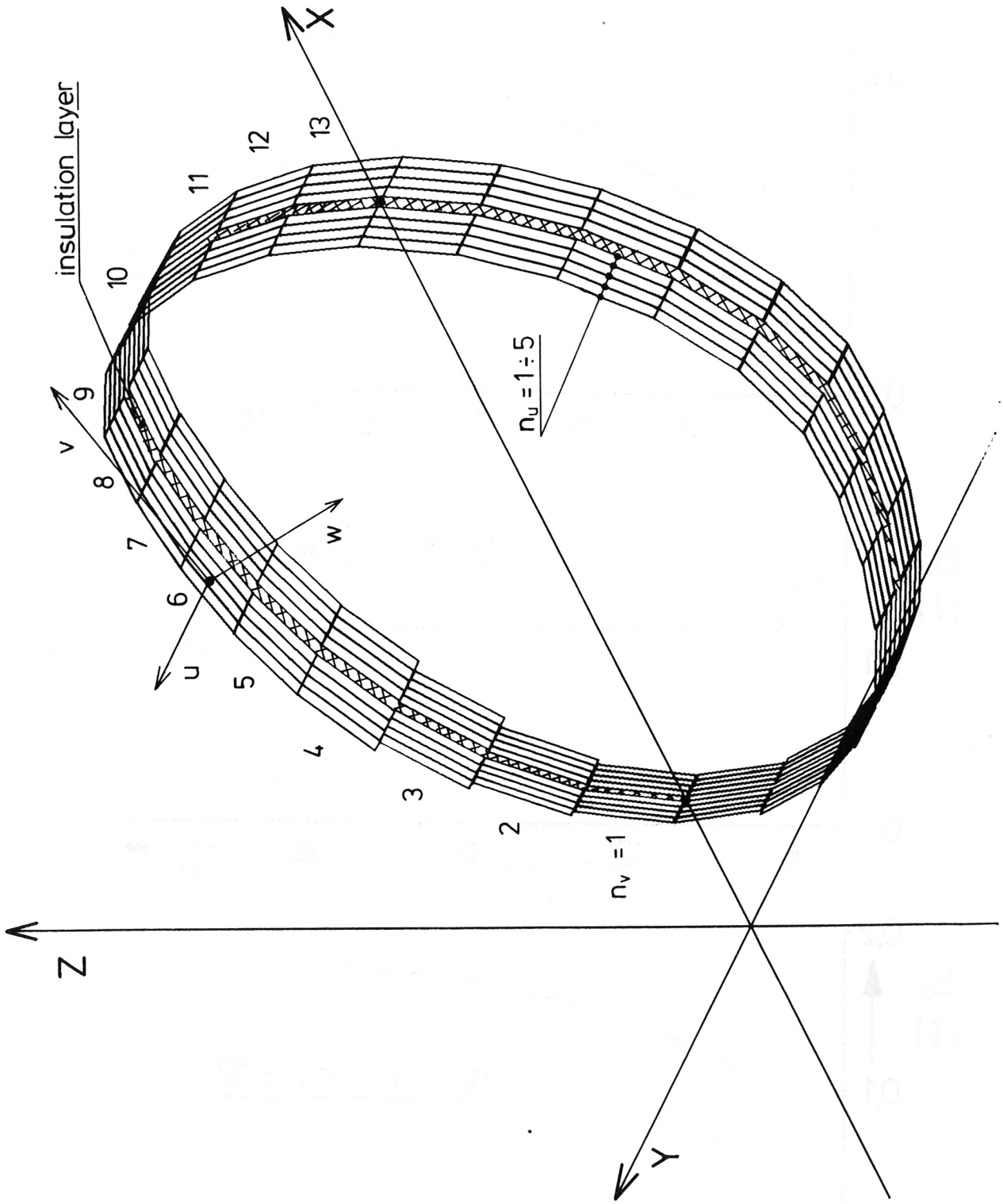

Fig. 22: Distribution of the u-plates in both pancakes of a coil for $n_w = 1$.

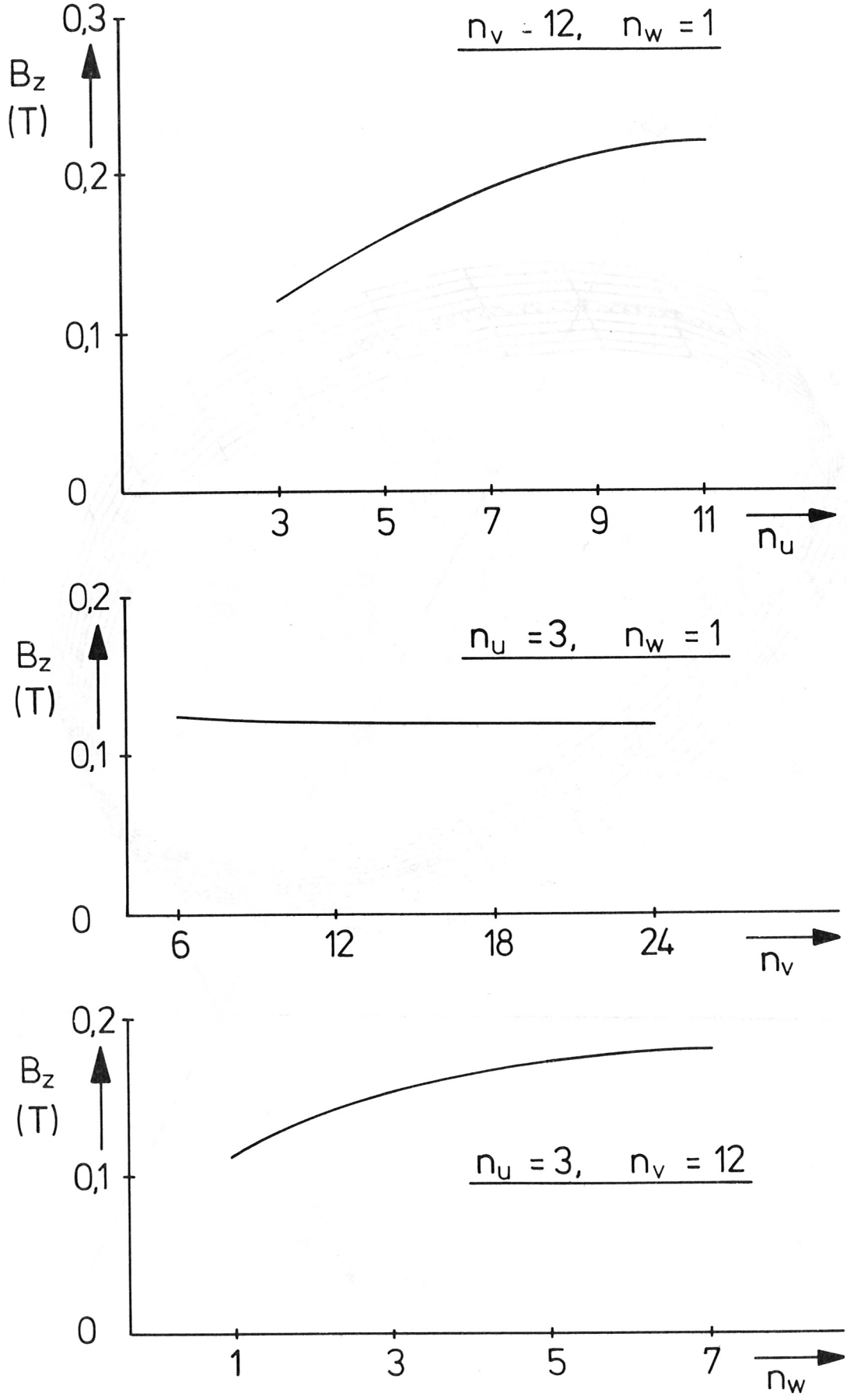

Fig. 23: Magnetic flux density produced by eddy currents at space point R = 1.15 m, $\varphi = 22.5^{\circ}$, Z = 0.

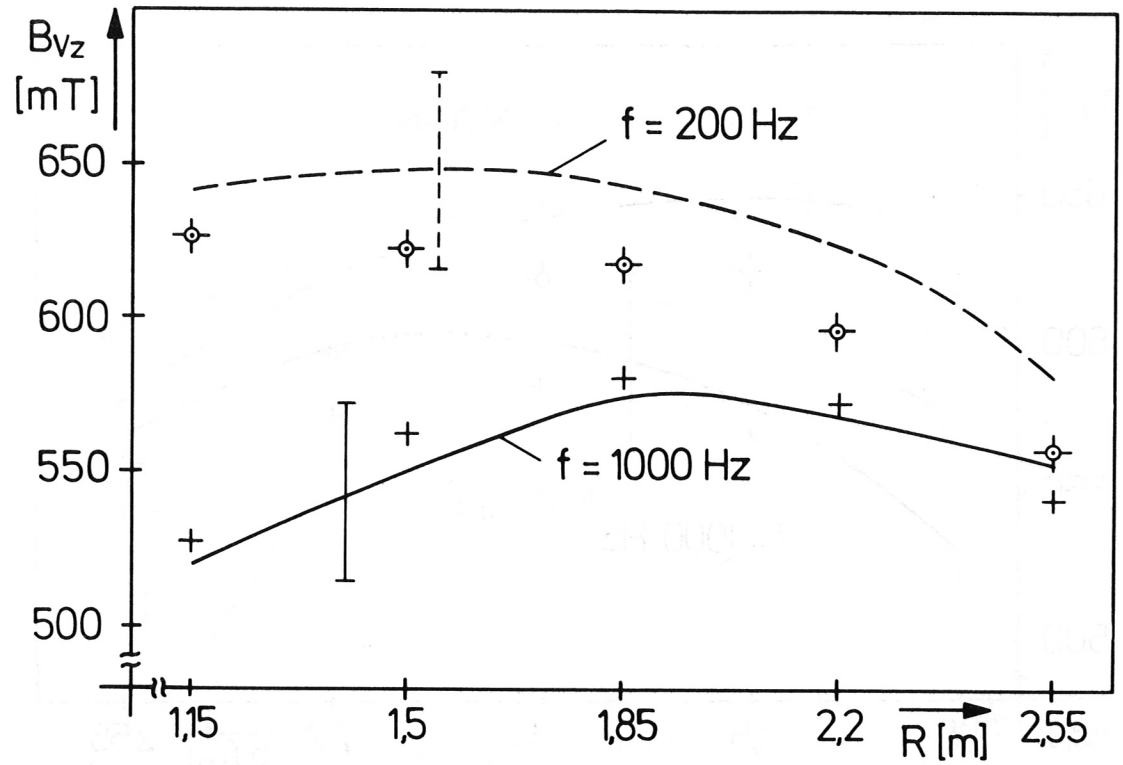

Fig. 24: Amplitude of B_{V_Z} for sinusoidal excitation of VF coils at the plane A-A, z = 0

f = 1000 Hz ——— measured

+ + + + calculated

f = 200 Hz ------- measured

-⊙- -⊙- calculated

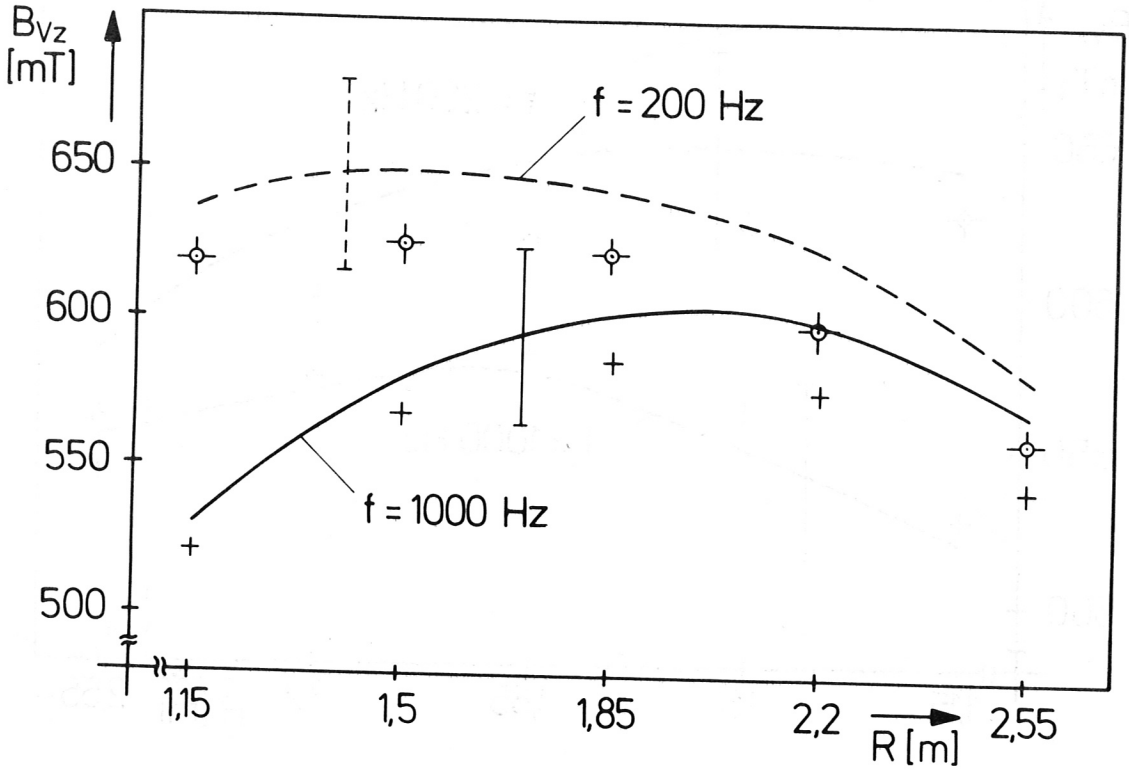

Fig. 25: Amplitude of B_{Vz} for sinusoidal excitation of VF coils at the plane A-A, z = 0.25 m

f = 1000 Hz ———— measured

\+ + + + + calculated

f = 200 Hz ---------- measured

⊕ ⊕ calculated

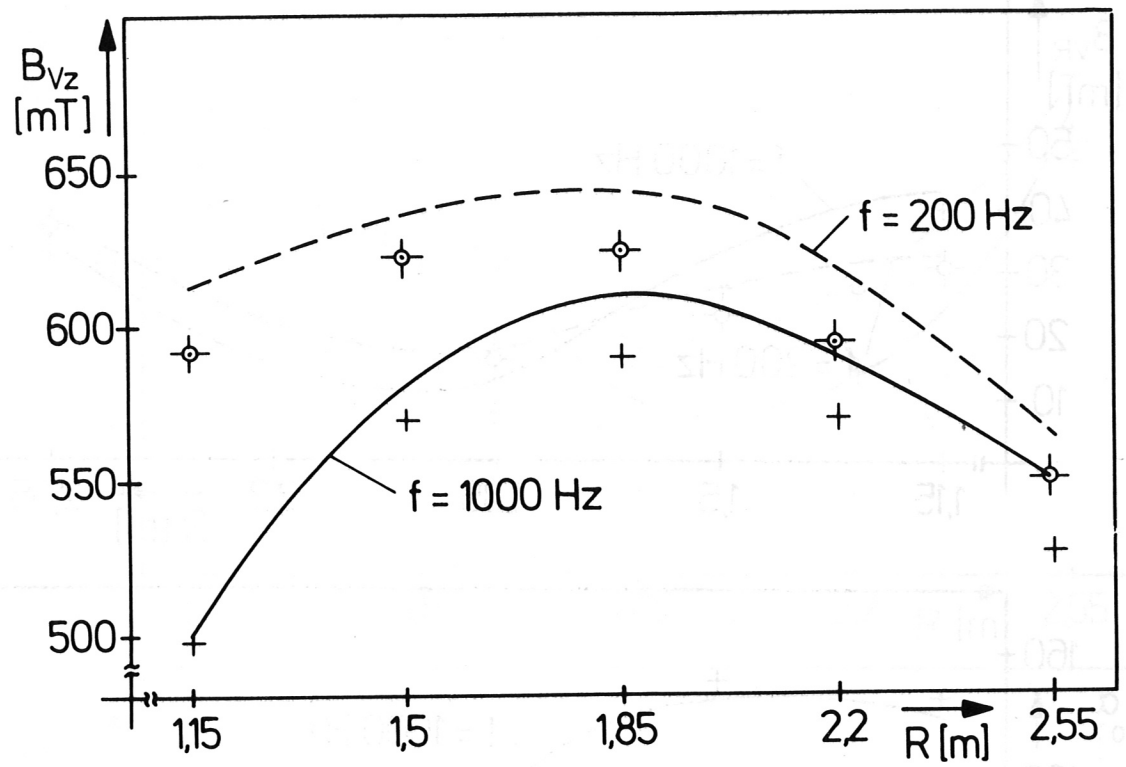

Fig. 26: Amplitude of B_{Vz} for sinusoidal excitation of VF coils at the plane A-A, z = 0.5 m

f = 1000 Hz ———— measured

+ + + + + + calculated

f = 200 Hz ---------- measured

⊙ ⊙ calculated

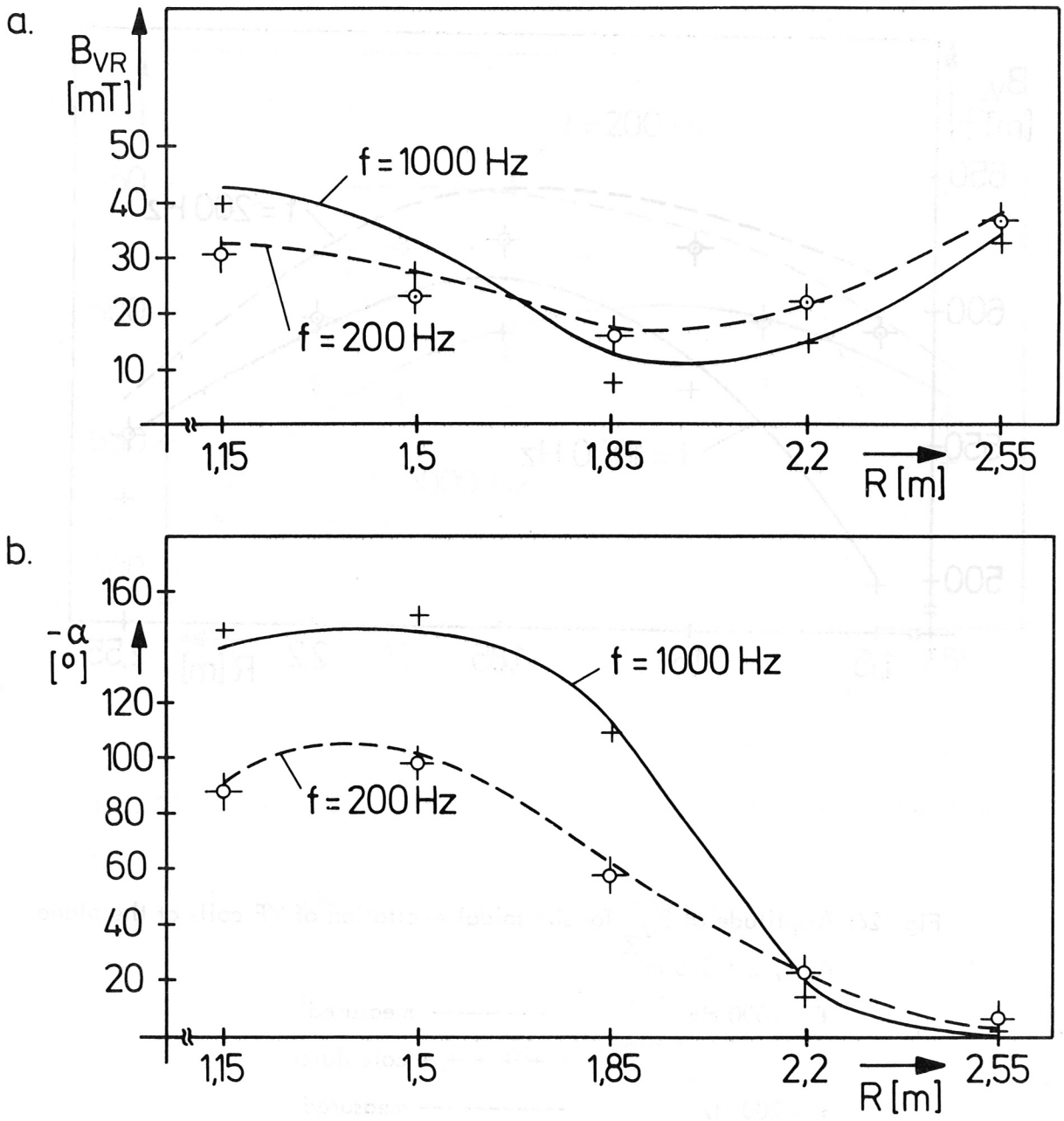

Fig. 27: a) Amplitude
b) Phase shift
of B_{V_R} for sinusoidal excitation of VF coils at the plane A-A, z = 0.25

f = 1000 Hz ——— measured
+ + + + calculated

f = 200 Hz - - - - - - - measured
⊕ ⊕ calculated

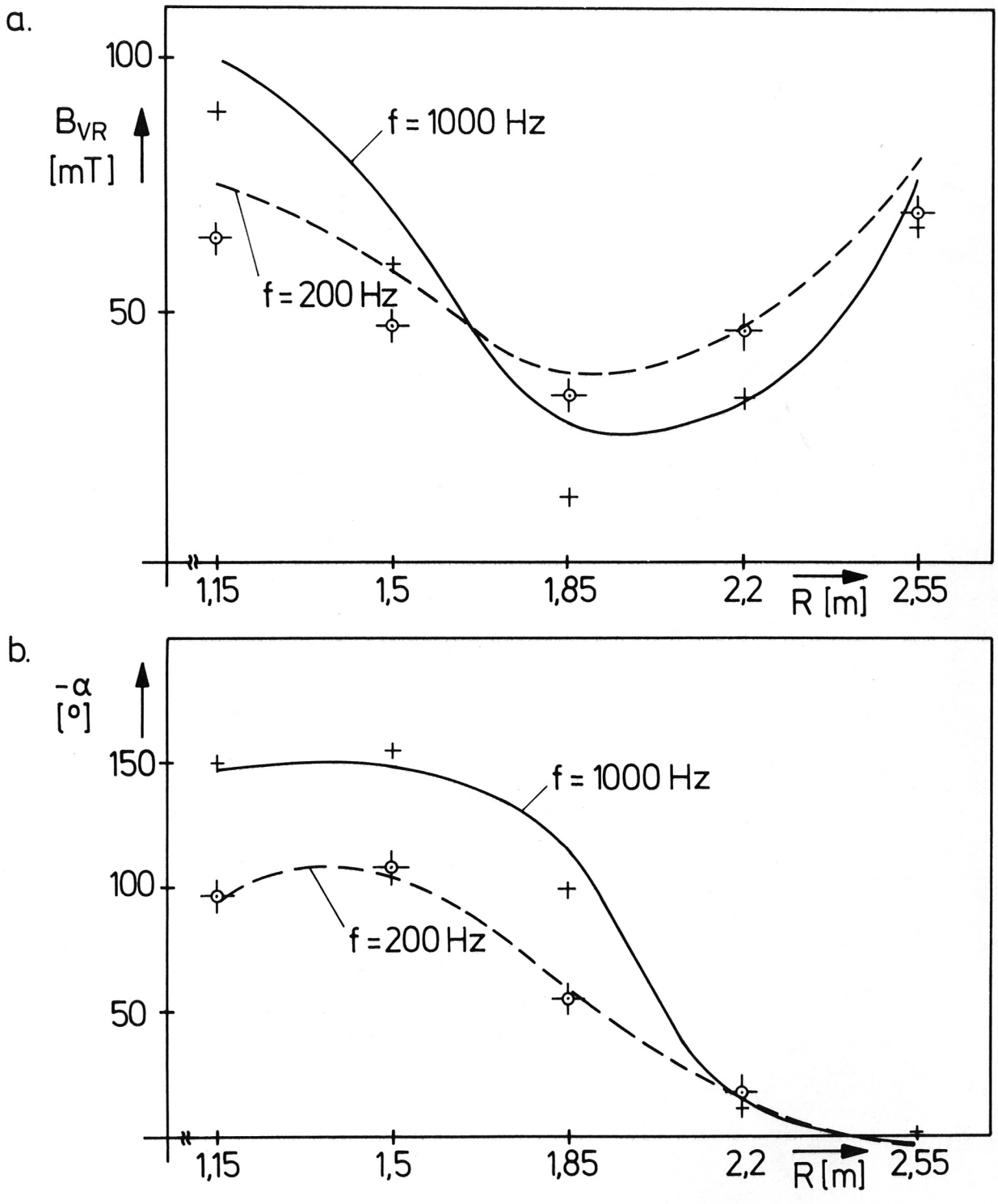

Fig. 28: a) Amplitude
b) Phase shift
of B_{V_R} for sinusoidal excitation of VF coils at the plane A-A, z = 0.5

f = 1000 Hz ——— measured
+ + + + calculated

f = 200 Hz - - - - - - - measured
⊙ ⊙ calculated